JOURNAL OF GEOPHYSICAL RESEARCH, VOL. 106, NO. D2, PAGES 1713–1732, JANUARY 27, 2001

Inorganic chlorine partitioning in the summer lower stratosphere: Modeled and measured [$ClONO_2$]/[HCl] during POLARIS

P. B. Voss,[1] R. M. Stimpfle,[1] R. C. Cohen,[1,2] T. F. Hanisco,[1] G. P. Bonne,[1,3] K. K. Perkins,[1] E. J. Lanzendorf,[1] J. G. Anderson,[1] R. J. Salawitch,[4] C. R. Webster,[4] D. C Scott,[4] R. D. May,[4] P. O. Wennberg,[5] P. A. Newman,[6] L. R. Lait,[6] J. W. Elkins,[7] and T. P. Bui[8]

Abstract. We examine inorganic chlorine (Cl_y) partitioning in the summer lower stratosphere using in situ ER-2 aircraft observations made during the Photochemistry of Ozone Loss in the Arctic Region in Summer (POLARIS) campaign. New steady state and numerical models estimate [$ClONO_2$]/[HCl] using currently accepted photochemistry. These models are tightly constrained by observations with OH (parameterized as a function of solar zenith angle) substituting for modeled HO_2 chemistry. We find that inorganic chlorine photochemistry alone overestimates observed [$ClONO_2$]/[HCl] by approximately 55-60% at mid and high latitudes. On the basis of POLARIS studies of the inorganic chlorine budget, [ClO]/[$ClONO_2$], and an intercomparison with balloon observations, the most direct explanation for the model-measurement discrepancy in Cl_y partitioning is an error in the reactions, rate constants, and measured species concentrations linking HCl and ClO (simulated [ClO]/[HCl] too high) in combination with a possible systematic error in the ER-2 $ClONO_2$ measurement (too low). The high precision of our simulation (±15% 1σ for [$ClONO_2$]/[HCl], which is compared with observations) increases confidence in the observations, photolysis calculations, and laboratory rate constants. These results, along with other findings, should lead to improvements in both the accuracy and precision of stratospheric photochemical models.

1. Introduction

The Photochemistry of Ozone Loss in the Arctic Region in Summer (POLARIS) campaign provided an unprecedented opportunity to examine the gas-phase photochemical reactions that control inorganic chlorine partitioning in the lower stratosphere. Three deployments in 1997 followed the evolution of the lower stratosphere from the early spring (April/May), through the summer (July/August), and into the fall (September). Instruments aboard NASA's ER-2 aircraft made the first in situ measurements of [$ClONO_2$] along with measurements of [HCl] and all other species necessary to model the partitioning ratio, [$ClONO_2$]/[HCl]. The observations extend upward to over 21 km in altitude and range from the tropics to the North Pole. The absence of appreciable heterogeneous chlorine chemistry during the campaign simplifies the analysis and strengthens the conclusions.

Analysis of the inorganic chlorine budget [*Bonne et al.*, 2000] and [ClO]/[$ClONO_2$] [*Stimpfle et al.*, 1999] complement the present work on partitioning. The budget analysis, which does not rely on rate constants or photolysis rates, constrains potential measurement errors in [HCl] and, to a lesser degree, [$ClONO_2$]. The [ClO]/[$ClONO_2$] study, in contrast, focuses on a subset of the rate constants, photolysis rates, and observed species concentrations that regulate [$ClONO_2$]/[HCl]. Remote spectroscopic observations of [HCl] and [$ClONO_2$] obtained by the MarkIV balloon instrument during POLARIS further contribute to our analysis. The balloon observations allow an intercomparison with the ER-2 measurements [*Toon et al.*, 1999] and also extend to greater altitudes [*Sen et al.*, 1999].

Understanding the gas-phase partitioning between HCl and $ClONO_2$ is fundamental to quantifying stratospheric ozone loss. These two species constitute more than 95% of inorganic chlorine ($Cl_y \approx ClONO_2$ + HCl + ClO + Cl + HOCl + ClOOCl) throughout most of the lower stratosphere [*Rowland et al.*, 1976; *Bonne et al.*, 2000]. HCl is the more stable species and is essentially inert on a timescale of days. In contrast, $ClONO_2$ is rapidly photolyzed to produce Cl and ClO and therefore may be responsible for 25-30% of gas-phase ozone destruction at midlatitudes in the lower stratosphere

[1] Department of Chemistry and Chemical Biology, Harvard University, Cambridge, Massachusetts.
[2] Now at the Department of Chemistry and Department of Geology and Geophysics, University of California, Berkeley.
[3] Now at Applied Materials, Santa Clara, California.
[4] Jet Propulsion Laboratory, California Institute of Technology, Pasadena.
[5] Division of Geological and Planetary Sciences, California Institute of Technology, Pasadena.
[6] NASA Goddard Space Flight Center, Greenbelt, Maryland.
[7] NOAA Climate Monitoring and Diagnostics Laboratory, Boulder, Colorodo.
[8] NASA Ames Research Center, Moffett Field, California.

Paper number 2000JD900494.
0148-0227/01/2000JD900494$09.00

[*Wennberg et al.*, 1994a]. In the polar regions, heterogeneous conversion of HCl and $ClONO_2$ into ClO and its dimer during the winter and early spring can lead to even greater amounts of halogen-catalyzed ozone loss. The cumulative ozone destruction caused by these heterogeneous processing events is controlled in part by the gas-phase reactions examined in this paper.

Using the POLARIS observations, we address the following questions:

1. What factors control the gas-phase partitioning of inorganic chlorine in the lower stratosphere? Do the observations support the existence of secondary processes that modify the primary control by $[O_3]$ and $[CH_4]$?
2. Are currently accepted rate constants and photolytic cross sections consistent with observations of $[ClONO_2]$, [HCl], $[O_3]$, $[CH_4]$, and [OH]? Can errors in our understanding of Cl_y partitioning be attributed to particular reactions, photolysis rates, measurements, and/or parcel trajectories?
3. What is the dominant source of scatter in model-measurement regressions for $[ClONO_2]/[HCl]$? Can reductions in scatter provide information on the accuracy of model inputs such as back trajectories and the reaction set?
4. How rapidly do $ClONO_2$ and HCl repartition? What parameters control the partitioning lifetime?
5. Are discrepancies in our current understanding of gas-phase Cl_y partitioning important to ozone loss processes? How will chlorine-catalyzed ozone loss respond to changes in stratospheric temperature and trends in halogen, methane, reactive nitrogen, and water vapor concentration?

Our analysis is based on the photochemical reactions reported in JPL97 [*DeMore et al.*, 1997] and the ~6% production of HCl from the reaction OH+ClO [*Lipson et al.*, 1997]. On the basis of the photochemical reactions of JPL97 as implemented in the JPL PSS model (see below), we neglect species that are believed to constitute less than 2% of total inorganic chlorine (e.g., HOCl, Cl_2O_2) and reactions that have less than a 1% effect on $[ClONO_2]/[HCl]$ (e.g., $ClONO_2+H_2O$ on sulfate aerosols in the comparatively warm conditions encountered during the summer). The resulting DeMore-Lipson inorganic chlorine reaction set is listed as (R1)-(R19) in Table 1. Whenever appropriate, we discuss the impact of the updated rates (reactions (R4), (R5), (R8), and (R9)) from JPL00 [*Sander et al.*, 2000].

Three different models are used in the analysis. The first of these, a Tau Averaged Steady State Partitioning (TASSP) approximation for $[ClONO_2]/[HCl]$, is developed in section 3 of this paper. This approximation uses time constants to convert a standard Instantaneous Steady-State (ISS) approximation into a diurnally averaged expectation value. It is based on the linear set of reactions (R1)-(R8) in Table 1 (black reactions in Figure 1). HO_x chemistry is replaced with [OH] observations that are parameterized as a function of solar zenith angle (see section 2.3). The TASSP approximation is used to propagate errors, highlight the factors that control inorganic chlorine partitioning, and guide the interpretation of more complete models. The new steady state methodology developed in section 3 should prove useful beyond the present analysis.

A more complete model, referred to as the Augmented Reaction Set Numerical Integration Partitioning (ARSNIP) model, is covered in section 4. This model achieves a balance between completeness and simplicity: it is accurate while still allowing us to examine the chemistry of inorganic chlorine partitioning in isolation (i.e., [OH] is parameterized as it is in the TASSP approximation). The ARSNIP model is based on the reaction set (R1)-(R19) in Table 1 and is illustrated in Figures 1 and 2.

A third model, the Jet Propulsion Laboratory Photochemical Steady-State (JPL PSS) model (NASA ER-2 POLARIS archive [*Salawitch et al.*, 1994a]) is used primarily to verify the accuracy of the ARSNIP model. The JPL PSS model assumes that the 24-hour average production and loss rates for all calculated species achieve equilibrium for the conditions

Table 1. Chemical Reaction Set for the TASSP and ARSNIP Models

Reaction		TASSP Approximaton		ARSNIP Model	
		Production	Loss	Production	Loss
(R1)	$ClONO_2 + hv \rightarrow Cl + NO_3$; $ClO + NO_2$	ClO	$ClONO_2$	Cl	$ClONO_2$
(R2)	$ClO + NO_2 + M \rightarrow ClONO_2 + M$	$ClONO_2$	ClO	$ClONO_2$	ClO
(R3)	$ClO + NO \rightarrow Cl + NO_2$	Cl	ClO	Cl, NO_2	ClO, NO
(R4)	$Cl + O_3 \rightarrow ClO + O_2$	ClO	Cl	ClO	Cl
(R5)	$Cl + CH_4 \rightarrow HCl + CH_3 \rightarrow \ldots HCl + H_2CO$	HCl	Cl	HCl, H_2CO	Cl
(R6)	$HCl + OH \rightarrow Cl + H_2O$	Cl	HCl	Cl	HCl
(R7)	$NO_2 + hv \rightarrow NO + O$	NO	NO_2	NO	NO_2
(R8)	$NO + O_3 \rightarrow NO_2 + O_2$	NO_2	NO	NO_2	NO
(R9)	$ClO + OH \rightarrow HCl + O_2$ (6%)			HCl	ClO
	$\rightarrow Cl + HO_2$ (94%)			Cl	ClO
(R10)	$Cl + H_2 \rightarrow HCl + H$			HCl	Cl
(R11)	$Cl + C_2H_6 \rightarrow HCl +$ products			HCl	Cl
(R12)	$Cl + H_2CO \rightarrow HCl + HCO$			HCl	Cl
(R13)	$O^1D + CH_4 \rightarrow \ldots H_2CO$			H_2CO	
(R14)	$OH + CH_4 \rightarrow \ldots H_2CO$			H_2CO	
(R15)	$H_2CO + hv \rightarrow$ products				H_2CO
(R16)	$H_2CO + OH \rightarrow$ products				H_2CO
(R17)	$O_3 + hv \rightarrow O^1D + O_2$			O^1D	
(R18)	$O^1D + O_2 \rightarrow O^3P + O_2$				O^1D
(R19)	$O^1D + N_2 \rightarrow N_2O$				O^1D

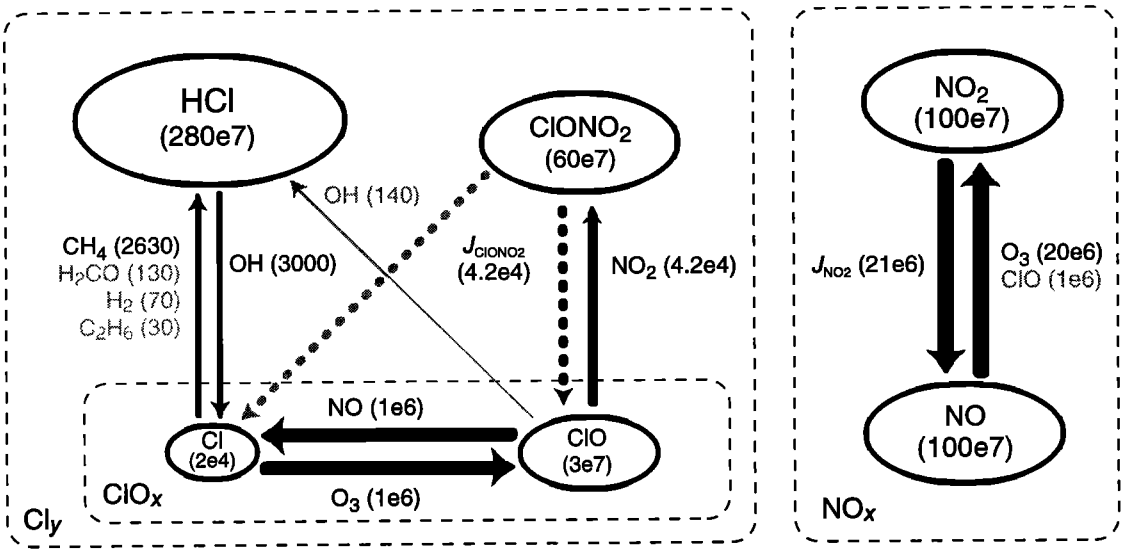

Figure 1. Inorganic chlorine partitioning in the summer lower stratosphere. Approximate reaction rates (molecule cm^{-3} sec^{-1}) and reservoir sizes (molecule cm^{-3}) are based on mid-day observations at cruise altitude (P<80 mbar). Black arrows and reactions denote the linear reaction set used in both the TASSP approximation and the ARSNIP model. Reactions shown in gray are used in the ARSNIP model only. The photolysis of $ClONO_2$ produces ClO in the TASSP approximation and Cl in the ARSNIP model. NO_x and Cl_y partitioning are coupled through the reactions ClO+NO and ClO+NO_2.

(e.g., latitude, temperature, pressure, etc.) of the sampled air mass. It includes approximately 35 species and 220 chemical reactions and is not constrained by parameterized OH. This model has been used extensively to examine measurements from balloon [e.g., *Sen et al.*, 1999], satellite [e.g., *Michelsen et al.*, 1996], and aircraft platforms [e.g., *Wennberg et al.*, 1999].

2. Observations and Derived Quantities

Relevant units and symbols are listed in Table 2.

2.1. ER-2 Observations

Twenty-one flights originated from Fairbanks, Alaska (65°N, 147°W), two from Moffett Field, California (37°N, 122°W), and two from Barber's Point, Hawaii (21°N, 158°W). Flights ranged in latitude from 3°S to 90°N with approximately 85% of the observations concentrated between 65°N and 90°N. Tropospheric observations are excluded by limiting analysis to [CO] less than $5x10^{10}$ molecule/cm^3 and pressure less than 93 mbar.

In situ observations of [$ClONO_2$] were made using a new

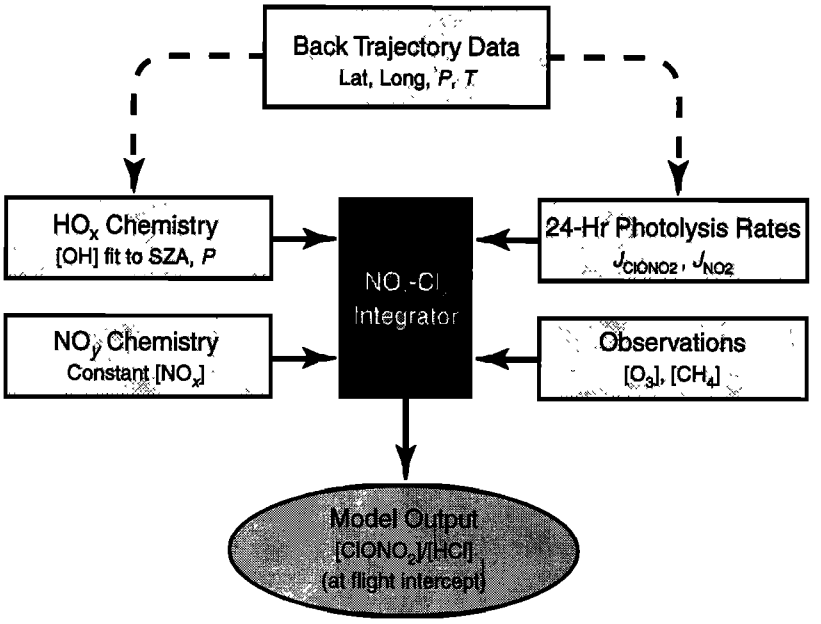

Figure 2. Schematic diagram of the ARSNIP model that shows the primary inputs and outputs. Solid arrows denote inputs for all model versions, while dashed arrows show inputs for the trajectory version only.

Table 2. Symbols and Units

Symbol	Description	Units
[X]	concentration of species X	molecule cm^{-3}
J_X	photolysis rate of species X	$seconds^{-1}$
k_{X1+X2}	rate constant (X1+X2→products)	$cm^3\ s^{-1}$
τ	time constant	seconds
SZA	solar zenith angle	degrees
T	temperature	Kelvins
P	pressure	mbar

thermal dissociation/resonance fluorescence instrument. This instrument employs resistively heated silicon strips to raise the sample air temperature to approximately 515 K. As the air flows to the detection axis (~10 ms downstream), $ClONO_2$ molecules thermally dissociate to produce ClO and NO_2 fragments. Injectors in the airstream add excess NO, converting the ClO fragments into Cl atoms with approximately 90% efficiency. At the detection axis the concentration of Cl is measured by resonance fluorescence. Thus the increase in the chlorine atom signal when the heater is turned on provides a measure of $[ClONO_2]$ in the sample airstream. With the exception of the silicon heater and new lightweight hardware, this instrument is nearly identical to the previous ER-2 ClO instrument that it replaced [*Brune and Anderson,* 1989]. Additional details of the $ClONO_2$ experiment are provided by *Bonne et al.* [2000].

Table 3 lists the reported accuracy of the observations used in our analysis. Observations of $[O_3]$, $[CH_4]$, [NO], $[NO_2]$, $[N_2O]$, $[ClONO_2]$, and [HCl] are averaged over periods of ±60 s at approximately 2-min intervals along the flight tracks. The time grid is chosen to match that used in the JPL PSS model (NASA ER-2 POLARIS archive [*Salawitch et al.,* 1994a]). The spacing of the time grid ranges from 1-3 min, with a greater density of points covering regions where the aircraft is changing altitude, traversing the day/night terminator, or encountering strong gradients in tracer concentrations.

The concentration of C_2H_6 (a minor contributor to HCl production) is estimated using its correlation with N_2O from the Atmospheric Trace Molecule Spectroscopy Experiment (ATMOS) instrument [*Rinsland et al.,* 1987]. The H_2 mixing ratio (also a minor contributor to HCl production) is set to 0.5 ppmv based roughly on the observations [*Elkins et al.,* 1996]. The concentration of NO_x, which has only a small effect on Cl_y partitioning, is calculated as the sum of observed [NO] and the geometric mean of the Harvard and National Oceanic and Atmospheric Administration (NOAA) $[NO_2]$ measurements. If either the NO or NO_2 measurement is absent in an averaging interval, then $[NO_x]$ and the missing species are estimated using a steady state approximation (reactions (R3), (R7), and (R8) in Table 1 with a small correction factor that is different for each deployment) [see also *Del Negro et al.,* 1999].

In the TASSP and ARSNIP models (and, by extension, in the JPL PSS model), the uncertainty in simulated $[ClONO_2]/[HCl]$ is dominated by the propagated uncertainty of the measurements (accuracies reported in Table 3), rate constants, and photolysis rates. Uncertainty in the model output due to the precision of these inputs is negligible in comparison.

2.2. Photolysis Rate Calculations

Photolysis rates (J_{ClONO2}, J_{NO2}, J_{O3}, and J_{H2CO}) are calculated using a radiative transfer model with Rayleigh scattering [*Prather,* 1981; *Salawitch et al.,* 1994b]. Refraction and extinction of light by aerosols are not included in the calculation. These processes tend to cancel, and furthermore, they are only important at large solar zenith angles [*Wennberg et al.,* 1999] and therefore do not appreciably influence Cl_y partitioning.

When modeling species with short time constants (i.e., $[ClO]/[ClONO_2]$), photolysis rates are calculated using reflectivity measurements from the Composition and Photodissociative Flux Measurement (CPFM) instrument on board the ER-2. Cloud height is set to ground level for albedos <0.08, measured Total Ozone Mapping Spectrometer (TOMS) version 7 cloud height for albedos >0.8, and interpolated for albedos between these limits.

Photolysis rates calculated using the CPFM albedo are also used for modeling long-lived species (i.e., $[ClONO_2]/[HCl]$) in order to demonstrate the detrimental effect of this common

Table 3. POLARIS in Situ Observations

Species	Detection Method	Reference	Accuracy
$ClONO_2$	thermal dissociation resonance fluorescence	*Bonne et al.* [2000]	±20%
HCl	laser absorption spectroscopy	*Webster et al.* [1994b]	±10%
ClO	resonance fluorescence	*Brune and Anderson* [1989]	±17%
Cl_y	gas chromatography / tracer relations	*Elkins et al.* [1996]	±4%
O_3	UV absorption	*Proffitt and McLaughlin* [1983]	±5%
CH_4	laser absorption spectroscopy	*Webster et al.* [1994b]	±10%
CH_4	gas chromatography	*Elkins et al.* [1996]	±3%
OH	laser-induced fluorescence	*Wennberg et al.* [1994b]	±13%
NO	chemiluminescence	*Fahey et al.* [1989]	±6%
NO_2	laser-induced fluorescence	*Perkins et al.* [2001]	±10%
NO_2	photolysis / chemiluminescence	*Del Negro et al.* [1999]	±15-30%
N_2O	laser absorption spectroscopy	*Webster et al.* [1994b]	±5%
H_2	gas chromatography	*Elkins et al.* [1996]	± 6%
Pressure	pressure sensor	*Scott et al.* [1990]	±0.3 mbar
Temperature	temperature sensor	*Scott et al.* [1990]	±0.3 K
O_3 above	spectroradiometer	*McElroy* [1995]	±3%

practice. In general, however, the photolysis rates used in our TASSP and ARSNIP models are based on zonally averaged TOMS reflectivity measurements binned by latitude (5° increments) and by season (deployment). These climatological photolysis rates assume a fixed cloud height of 590 mbar.

All photolysis rates at a particular point along the ER-2 flight track are calculated using the same ozone profile. Ozone profile climatology (as a function of latitude and month) is derived from ER-2, satellite, and ozonesonde observations. The profiles are scaled to match CPFM measurements of the ozone column above the ER-2 and TOMS measurements of the total ozone column.

An alternate calculation of the photolysis rates [*Swartz et al.*, 1999] differs in its method of estimating the ozone profile and by its inclusion of refraction and extinction of light by aerosols. Because gas-phase Cl_y partitioning is relatively insensitive to these factors, the photolysis rates calculated by the methods of *Salawitch et al.* [1994b] and *Swartz et al.* [1999] produce nearly identical results when used in models that simulate $[ClONO_2]/[HCl]$. We use the photolysis rates provided by Salawitch for continuity with our earlier work.

2.3. [OH]-SZA Parameterization

A parameterization of observed [OH] replaces modeled HO_x photochemistry in both the TASSP and ARSNIP models (but not in the JPL PSS model). This parameterization ties our analysis directly to the observations, eliminating the coupling of HO_x and Cl_y chemistry that often confounds model-measurement comparisons.

The OH parameterization is based on the nearly linear variation of [OH] with solar zenith angle observed during POLARIS and, previously, during Airborne Southern Hemispheric Ozone Experiment / Measurements for Assessing the Effects of Stratospheric Aircraft (ASHOE/MAESA), the Stratospheric Photochemistry, Aerosols, and Dynamics Expedition (SPADE), and Stratospheric Tracers of Atmospheric Transport (STRAT) [*Hanisco et al.*, 2001; *Wennberg et al.*, 1994a]. This linear relationship occurs because OH production is proportional to $[O_3]$ and J_{O3} while OH loss is proportional to $[NO_y]$. Since $[O_3]$ and $[NO_y]$ are tightly correlated in these data sets [e.g., *Fahey et al.*, 1996], [OH] is proportional to J_{O3} only. Strong absorption by overhead ozone results in a near-linear variation of J_{O3} (and therefore OH production and concentration) with solar zenith angle (SZA) and, to a much lesser extent, with overhead ozone [*Hanisco et al.*, 2001].

We parameterize the POLARIS [OH] observations as a function of SZA in (1). Since overhead ozone induces only small deviations (<10%) in the linear OH-SZA relationship, it is replaced by the surrogate variable P (pressure in mbar).

$$[OH] = 55850\alpha - 84.6\alpha^2 - 440\alpha P$$
$$\alpha \equiv 94.5 - SZA. \quad (1)$$

The constants were determined by a least squares fit to the [OH]-SZA data with the approximate zero intercept, [OH]=0 at SZA=94.5°, determined by visual inspection. [OH] is always constrained to be non negative.

Parameterized [OH] from (1) is compared with observed [OH] over the full range of daytime solar zenith angles in Figure 3a. Figure 3b shows the fractional error in the parameterization. While estimated [OH] can be more than 50% in error for individual data points, the statistical confidence in the fit is high; when averaged over any moderate range of SZA, the error in the parameterization is generally less than 10%. Thus using parameterized [OH] in a diurnal model only moderately augments the $\pm 13\%$ 1σ uncertainty of the OH measurement.

3. Steady State Inorganic Chlorine Partitioning

3.1. Time Constants of Inorganic Chlorine Partitioning

Accurate time-constant calculations are fundamental to many aspects of our analysis including derivations that refine steady state approximations for $[ClONO_2]/[HCl]$ and $[ClO]/[ClONO_2]$. Typically, time constants are estimated as concentration divided by the rate of production or loss (equivalent to the pseudo first-order loss rate). While this method is valid for monotonically decaying source species such as the CFCs and N_2O, it is not accurate for non linear systems [*Prather*, 1994] or for systems where the source species is not decaying to zero (i.e., most steady state systems).

In Figure 4 we develop a generic model for estimating time constants that is applicable to many steady state systems including $ClONO_2$-ClO and $ClONO_2$-HCl. This AB-Reservoir (ABR) model is based on a primary pair of chemical species (A and B) that rapidly exchange with reservoir species (R_A and R_B) and slowly exchange with each other (via pseudo first-order reactions rates a and b). The ratios r_A and r_B denote $[R_A]/[A]$ and $[R_B]/[B]$, respectively. The time constant of the ABR system can be calculated explicitly from the system of first-order differential equations; the rapidly exchanging reservoirs add inertia to the system which can be treated as slowing the rates a and b by (r_A+1) and (r_B+1), respectively.

$$\tau_{ABR} \approx \frac{1}{a/(r_A+1) + b/(r_B+1)} \quad (2)$$

Specifically, τ_{ABR} is the time required for either [A] or [B] to relax to $1/e$ of its initial difference from steady state. It is accurate to within approximately 10% when both reservoir exchange rates exceed the A-B exchange rate $(a+b)$ by a factor of at least 5-10.

In the case of $ClONO_2$-ClO partitioning, there are no rapidly exchanging reservoirs, and the time constant is given by (3).

$$\tau_{ClO_x} \approx \frac{1}{k_{ClO+NO2}[NO_2] + J_{ClONO2}} \quad (3)$$

On the basis of observations at midlatitudes (60°-70°N), τ_{ClO_x} is approximately 15-30 min at midday and 5-15 min at sunrise and sunset. The time constant is longest at midday because the denominator of (3) is dominated by $k_{ClO+NO2}[NO_2]$, a term that decreases as NO_2 is photolyzed to NO. During the spring and summer, τ_{ClO_x} decreases as $[NO_x]$ (and therefore $[NO_2]$) increases under extended daylight). In the fall, low $[NO_x]$ and slower photolysis increase τ_{ClO_x} to almost an hour.

Estimating the time constant for $ClONO_2$-HCl partitioning is more complex. As shown in Figure 4b, HCl-Cl is selected as the primary pair, and ClO+$ClONO_2$ is selected as the reservoir R_B. Thus in equation (2) $a=k_{OH+HCl}[OH]$, $b=k_{Cl+CH4}[CH_4]$, $r_A=0$, and $r_B \approx [ClONO_2]/[Cl]$ (which is replaced by its steady state approximation (R1)-(R4); (R7)-(R8)) producing an ex-

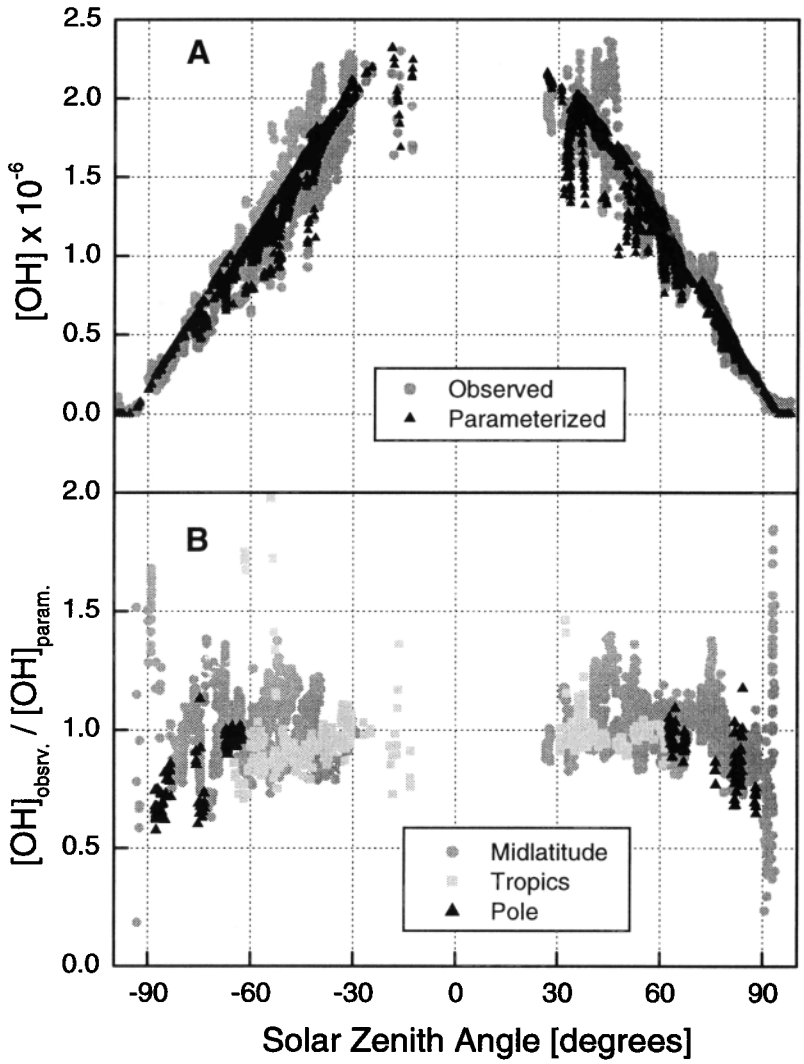

Figure 3. (a) POLARIS [OH] observations (gray) and the corresponding parameterization (black). (b) Fractional error in estimated [OH] as a function of solar zenith angle for the tropics (<40°N), midlatitudes (40°-80°N), and pole (>80°N).

plicit formula for the instantaneous $ClONO_2$-HCl time constant (4).

$$\tau_{Cly} \approx \left(\frac{k_{ClO+NO} k_{CH4+Cl} J_{ClONO2} J_{NO2} [CH_4]}{k_{ClO+NO2} k_{Cl+O3} k_{NO+O3} [O_3]^2} + k_{HCl+OH} [OH] \right)^{-1} \quad (4)$$

For typical midday conditions in the lower stratosphere, τ_{Cly} is approximately 5 days. Equation (4) agrees with the exact (and more complex) eigenmode calculation of *Prather* [1994] to within approximately 10%. The error in (4) grows to more than 25% in the lower tropical stratosphere because low ozone concentrations slow the reservoir exchange rate and therefore compromise the rapidly exchanging reservoir assumption of the ABR model. The significance of both terms in (4) (approximately 70% and 30%, respectively) exposes one reason that conventional first-order-loss methods fail to accurately predict partitioning time constants.

The time constant for Cl_y partitioning (4) is a function of solar zenith angle and therefore varies with the time of day. Its diurnal average, the lifetime, is calculated as the inverse of the 24-hour average of $1/\tau_{Cly}$. The lifetime for Cl_y partitioning is shown as a function of latitude and season in Figure 5. During the spring and summer the partitioning lifetime is approximately 10 days at the pole and 2 days at the equator. This trend is driven largely by gradients in $[O_3]$; the shortest lifetimes (~hours) occur in the lower tropical stratosphere (lowest $[O_3]$) as seen during aircraft dives. In the fall, low light intensity greatly increases the lifetime at high latitudes.

Numerical integrations confirm that ABR time constants accurately describe the response of individual species (e.g., HCl, $ClONO_2$, or ClO) to any perturbation. The time constant also represents the response of a ratio such as $[ClONO_2]/[HCl]$ to gradual change (e.g., trajectory motion and midday changes in solar zenith angle) and to larger perturbations after several *e*-foldings.

A number of factors may contribute to the erroneously long lifetimes reported in the literature. *Webster et al.* [1993], for example, estimate the lifetime for HCl recovery following a processing event to be approximately 90 12-hour days. In this calculation it appears that the Cl mixing ratio (0.015 parts per

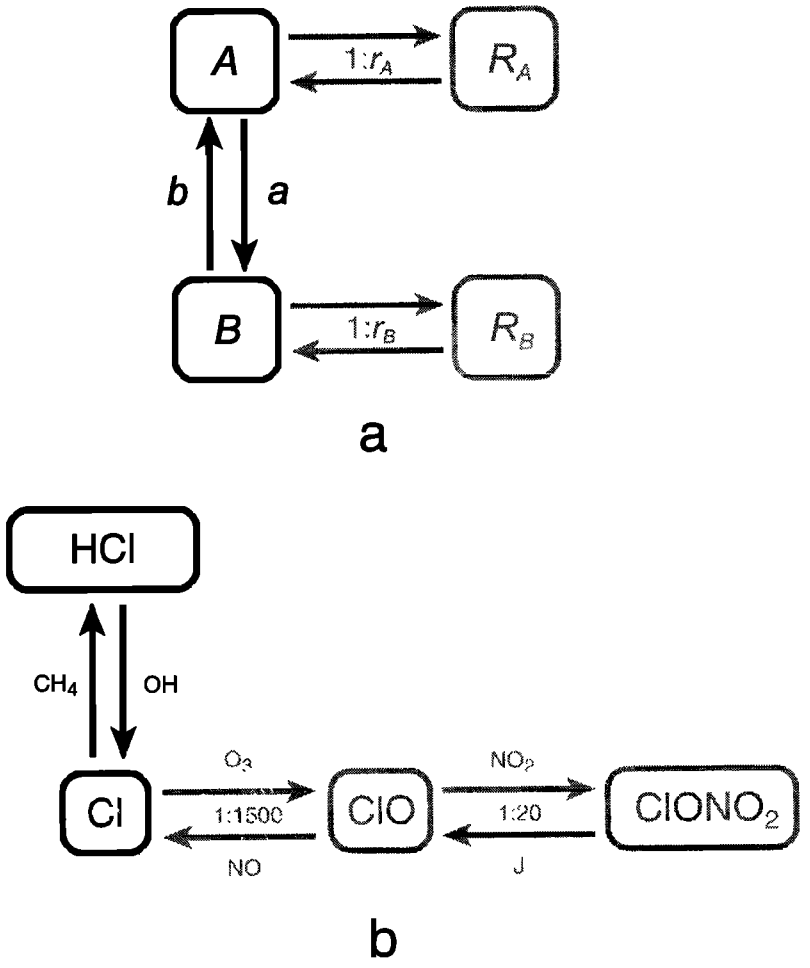

Figure 4. (a) Generic ABR model for estimating time constants (see text for details). (b) ABR model applied to Cl_y partitioning (ratios are approximate for midday).

trillion by volume (pptv)) is almost an order of magnitude too low for processed air and therefore inflates the lifetime by a similar amount. *Liu et al.* [1992] also report a long lifetime for HCl recovery (1-2 months). The authors point out that the recovery is limited by denitrification and is therefore controlled by the recovery of $[NO_x]$ rather than intrinsic properties of the inorganic chlorine system.

In summary, the lifetime for gas-phase inorganic chlorine partitioning is well described by (4) and is almost always in the range of 5-15 days. During the spring and summer there are no modes of inorganic chlorine partitioning that have a true 1-2 month lifetime.

3.2. Steady State for Short-Lived Species: $[ClO]/[ClONO_2]$

For systems that rapidly approach steady state (τ<hours) the time constant can account for chemistry that lags the solar zenith angle, providing a fundamental correction to the Instantaneous Steady-State (ISS) approximation. This correction significantly improves the approximation for $[ClO]/[ClONO_2]$, a central component of Cl_y partitioning.

The correction derives from a dynamic version of the ISS approximation. Traditional ISS assumes that $|P\text{-}L| << P$ (or L), where P and L are the respective production and loss rates of a species. Dynamic Steady State (DSS) meets the broader condition $|d/dt(P\text{-}L)| << |dP/dt|$, or equivalently, $P\text{-}L \approx C$ where C is any constant.

The DSS approximation, (5), is a function of the ISS approximation X_{ISS} and the time constant τ. The time constant is calculated using either the ABR equation (2) or the eigenmode method of *Prather* [1994].

$$X_{DSS} \approx X_{ISS} - \tau \frac{dX_{ISS}}{dt} \tag{5}$$

The derivation of (5) assumes that the exact solution $X(t)$ has the same time derivative as $X_{ISS}(t)$ and differs from it by a constant $\mathcal{E}$. Under these conditions it is straightforward to show that $\mathcal{E}=\tau dX_{ISS}(t)/dt$. In (5), $X_{DSS}(t)$ approximates $X(t)$ by subtracting $\mathcal{E}$ from $X_{ISS}(t)$. The derivation assumes that X represents a single species rather than a ratio of two species (a species in a two-component system always decays exponentially toward steady state while a ratio does not). Because the DSS correction is generally small (<30%), (5) is a good approximation for both single species and ratios.

Equations (6)-(8) show the first order DSS approximation for the ratio $[ClO]/[ClONO_2]$. The time constant in (6) is given by (3), while the conventional steady-state approximation for $[ClO]/[ClONO_2]$ and its time derivative are given by

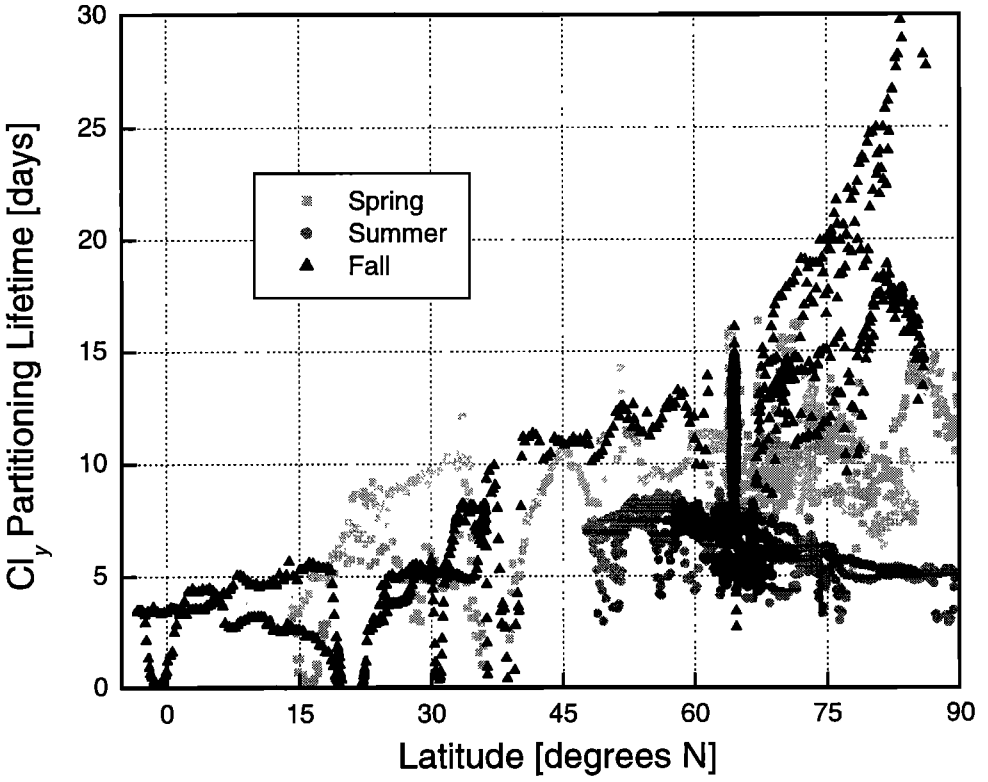

Figure 5. Lifetime (i.e., diurnal average time constant) for $ClONO_2$-HCl partitioning based on equation (4) and POLARIS observations (P<93 mbar) during the spring (April/May), summer (July/August), and fall (September).

(7) and (8), respectively. Primes denote derivatives with respect to time.

$$\left(\frac{[ClO]}{[ClONO_2]}\right)_{DSS} \approx \left(\frac{[ClO]}{[ClONO_2]}\right)_{ISS} - \tau_{ClOx}\left(\frac{[ClO]}{[ClONO_2]}\right)'_{ISS} \quad (6)$$

$$\left(\frac{[ClO]}{[ClONO_2]}\right)_{ISS} \approx \frac{J_{ClONO2}}{k_{ClO+NO2}[NO_2]} \quad (7)$$

$$\left(\frac{[ClO]}{[ClONO_2]}\right)'_{ISS} = \frac{J'_{ClONO2}}{k_{ClO+NO2}[NO_2]} + \frac{J_{ClONO2}J'_{NO2}([NO]+[NO_2])}{k_{ClO+NO2}k_{NO+O3}[NO_2][O_3]}\left(1+\frac{J_{NO3}}{k_{NO+O3}[O_3]}\right)^{-2} \quad (8)$$

Evaluation of (6)-(8) requires only instantaneous quantities: photolysis rates and their derivatives, rate constants, and species measurements. In general, dynamic steady state is applicable to systems that track diurnal change without long-term memory effects. The approximation becomes valid 3-5 e-foldings after sunrise and tracks the system until sunset.

3.3. Steady State for Long-Lived Species: [$ClONO_2$]/[HCl]

In the atmosphere and in numerically integrated models, long-lived species (τ>days) average the diurnal variation in the forcing conditions, achieving approximately constant concentrations throughout the day. This average, however, is heavily weighted toward the midday value of the Instantaneous Steady State (ISS) approximation, reflecting the faster photochemistry at small solar zenith angles. In (9) we estimate the expectation value $\langle X\rangle$ of an ISS approximation X_{ISS}, using the equilibration rate $1/\tau$ as a weighting function in the 24-hour average (denoted by overbars). Throughout the paper, this process is referred to as "τ-averaging."

$$\langle X\rangle \approx \frac{\overline{1/\tau\, X_{ISS}}}{\overline{1/\tau}} \quad (9)$$

The derivation of (9) assumes that X represents a single species rather that a ratio of two species. When applying (9) to a ratio, singularities and near singularities in X_{ISS} (generally at large solar zenith angles and at night) must be excluded from the average. We calculate the averages in (9) over the daytime hours where SZA<85°.

The ISS approximation for [$ClONO_2$]/[HCl] can be derived as a product of three separate ratios (10), each of which can be estimated using the linear reaction set, (R1)-(R8) [*Dessler et al.*, 1995]. Reactions that are of minor importance in the lower stratosphere (e.g., Cl+C_2H_6, ClO+OH, and NO+ClO) are accounted for later using a constant multiplier.

$$\left(\frac{[ClONO_2]}{[HCl]}\right)_{ISS} \approx \left(\frac{[ClONO_2]}{[ClO]}\frac{[ClO]}{[Cl]}\frac{[Cl]}{[HCl]}\right)_{ISS} \approx \left(\frac{k_{HCl+OH}k_{Cl+O3}k_{ClO+NO2}k_{NO+O3}}{k_{CH4+Cl}k_{ClO+NO}}\right) \times \left(\frac{[OH]}{J_{ClONO_2}J_{NO_2}}\right)\left(\frac{[O_3]^2}{[CH_4]}\right). \quad (10)$$

The three terms on the right-hand side of (10) control the partitioning ratio $[ClONO_2]/[HCl]$. These are as follows:

Rate term $K \equiv k_{HCl+OH} k_{Cl+O3} k_{ClO+NO2} k_{NO+O3} / k_{CH4+Cl} k_{ClO+NO}$

Insolation term $[OH]/(J_{ClONO2} J_{NO2})$

Tracer term $[O_3]^2/[CH_4]$

Because of its large dynamic range in the atmosphere, the tracer term exerts dominant control over inorganic chlorine partitioning (see section 3.4). The tracer term is approximately constant over the diurnal cycle and scales monotonically with pressure (e.g., along back trajectories). The rate constant and insolation terms exert secondary control, inducing smaller changes in $[ClONO_2]/[HCl]$.

When estimated using JPL97, the rate constant term is a linear function of pressure (dominated by the strong pressure dependence of the three body reaction $ClO+NO_2+M \rightarrow ClONO_2+M$). The absence of significant temperature dependence is due to a cancellation of the temperature dependencies in k_{NO+O3} and k_{Cl+CH4} (both with E/R=1400) and a similar, but not as complete, cancellation of the temperature dependencies in k_{Cl+O3}, k_{HCl+OH}, $k_{ClO+NO2}$, and k_{ClO+NO}. As discussed in section 3.4, observations indicate that, contrary to JPL97, K is function of temperature as well as pressure. JPL00 rate constants produce similar results.

The insolation term is controlled almost entirely by photolytic processes and is the most complex component of (10). It is highly sensitive to albedo because both J_{NO2} and J_{ClONO2} depend on albedo while [OH] does not (see equation (1)). The insolation term is much less sensitive to SZA and overhead ozone due to a partial cancellation between [OH] (driven by SZA and overhead ozone) and J_{ClONO2} (also driven by SZA and overhead ozone). The cancellation, however, is not complete and the insolation term does change appreciably during the day. The insolation term in (10) must therefore be τ-averaged to provide a reliable estimate of $[ClONO_2]/[HCl]$.

The τ-average of the insolation term is denoted by F in equation (11). Because $ClONO_2$ and HCl are decoupled at night (when radical species decay to zero), it is sufficient to average only over the day. F is relatively insensitive to the averaging cutoff solar zenith angle in the range of 85°-90°.

$$F \equiv \frac{1}{1/\tau}\overline{\left(\frac{1/\tau[OH]}{J_{ClONO2} J_{NO2}}\right)} \qquad (11)$$

Using (1), (4), and 24-hour photolysis rates, F can be evaluated explicitly. Because the insolation term peaks at small solar zenith angles, F increases toward the equator and is greatest around the summer solstice. Latitudinal trends in albedo compound this solar exposure effect, causing F to increase by nearly 100% from the poles to the equator. This F gradient can leave a substantial imprint on Cl_y partitioning when air parcels are subjected to latitude excursions.

Substituting F into (10) produces an expression for $[ClONO_2]/[HCl]$ that closely approximates the quantitatively accurate ARSNIP model (reactions (R1)-(R19)). Over a 24-hour period under typical POLARIS conditions (flight of July 7, 1997, ~60°N latitude, ~70 mbar, ~220 K), (10) neglects approximately 15% of HCl-production (R9-R12) and 5% of Cl production (reaction (R1)). The absence of $ClO_x \rightarrow NO_x$ coupling (effect of (R3) on NO_x partitioning) in the derivation of (10) introduces a compensating error of approximately 5%. A second compensating error (also ~5%) results from the failure of (10) to account for the flush of $ClONO_2$ produced by ClO at sunset. These errors cause (10) to overestimate $[ClONO_2]/[HCl]$ by 10% (±4% 1σ) in comparison with the more complete ARSNIP model (model 4 in Table 6). To account for this known missing chemistry, (10) is scaled by 0.91 (1/1.10) to produce the Tau Averaged Steady State Partitioning (TASSP) approximation:

$$\left\langle \frac{[ClONO_2]}{[HCl]} \right\rangle \approx (0.91)(K(P,T))(F(\text{lat, day}))\left(\frac{[O_3]^2}{[CH_4]}\right)$$

$$\approx (0.91)\left(\frac{k_{HCl+OH} k_{Cl+O3} k_{ClO+NO2} k_{NO+O3}}{k_{CH4+Cl} k_{ClO+NO}}\right)$$

$$\times \left(\frac{1}{\overline{1/\tau}}\right)\overline{\left(\frac{1/\tau[OH]}{J_{ClONO2} J_{NO2}}\right)}\left(\frac{[O_3]^2}{[CH_4]}\right). \qquad (12)$$

Significant errors in (12) occur only when the NO_x mixing ratio is less than 400 pptv (due to high [ClO] and the inaccuracy of (12) under these conditions) and when the minimum solar zenith angle during the day is greater than 75° (due to the errors in τ-averaging at large SZA).

The utility of τ-averaging is evident when (12) is compared with earlier steady state approximations of $[ClONO_2]/[HCl]$. Whereas (12) applies quantitatively over almost the entire (gas-phase) lower stratosphere, prior derivations are either qualitative [i.e., *Dessler et al.*, 1995] or limited by fixed constants to a modest range of latitude and season [i.e., *Sen et al.*, 1999]. Because (12) is not restricted in these respects, it simulates latitudinal and seasonal trends in $[ClONO_2]/[HCl]$. Furthermore, τ-averaging can be applied, without modification, to ISS approximations that are more complete than (10) (e.g., reactions used by *Sen et al.* [1999]), producing predictive equations analogous to (12) that are accurate over a wide range of altitude, latitude, and season.

In order to quantify the effect of Cl_y partitioning on ozone destruction, we next derive an expression for [ClO] (13) based on (8) and the steady state approximation for $[NO]/[NO_2]$ (reactions (R3), (R7), and (R8) in Table 1). In the derivation (not shown), HCl and $ClONO_2$ are assumed to comprise all of Cl_y [*Bonne et al.*, 2000] and $(1+[ClONO_2]/[HCl])$ is approximated by the constant 1.20 which, based on observations, is valid to within ±6% 1σ. [ClO] is then estimated from $[ClONO_2]$ using (R1), (R2), (R7), and (R8) with the scaling constant increased to 1.23 to compensate for neglecting (R3). The complete expression for [ClO], (14), results from substituting (12) into (13). Equation (13) links [ClO] with inorganic chlorine partitioning while (14) shows how [ClO] responds to changes in lower stratospheric composition.

$$[ClO] \approx \left(\frac{[Cl_y]}{1.23}\right)\left(\frac{J_{ClONO2}(J_{NO2} + k_{NO+O3}[O_3])}{k_{ClO+NO2} k_{NO+O3}[O_3][NO_x]}\right)\left\langle \frac{[ClONO_2]}{[HCl]} \right\rangle \qquad (13)$$

$$[ClO] \approx (0.74)(J_{ClONO2}(J_{NO2} + k_{NO+O3}[O_3]))\left(\frac{k_{HCl+OH} k_{Cl+O3}}{k_{CH4+Cl} k_{ClO+NO}}\right)$$

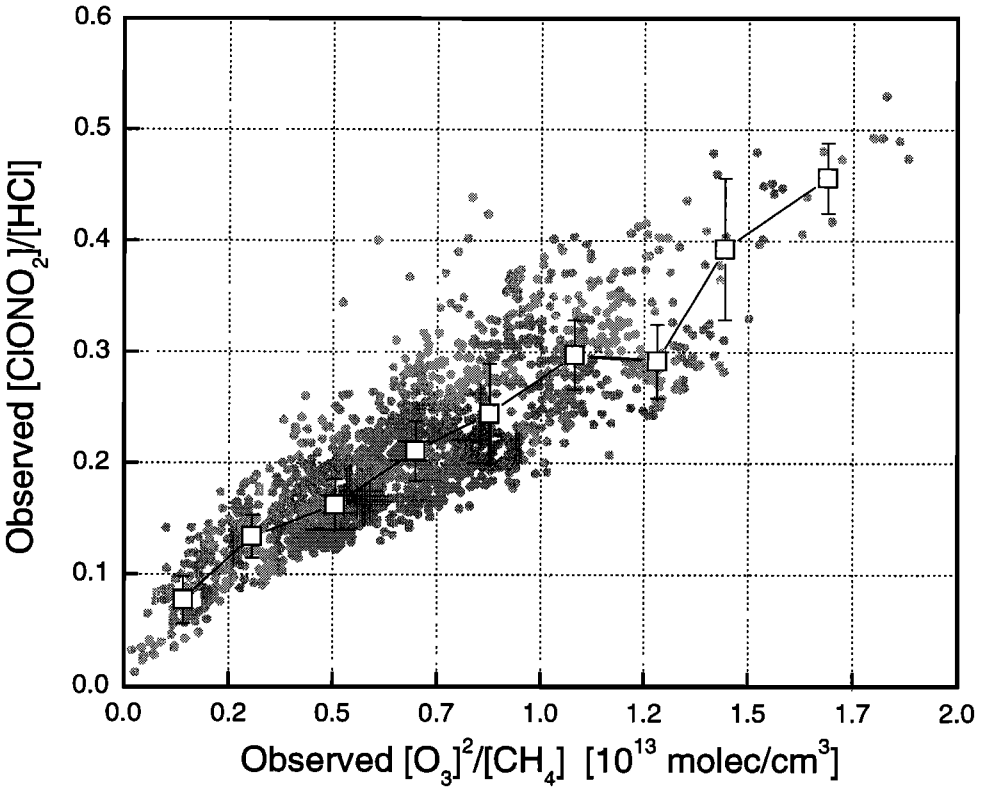

Figure 6. Inorganic chlorine partitioning as a function of $[O_3]^2/[CH_4]$ at a fixed latitude (50°-70°N) and pressure (53-67 mbar). Scatter in the relationship is introduced by the secondary factors K and F in equation (12). Bin medians and interquartile ranges are superimposed on the data.

$$\times \left(\frac{1}{\overline{1/\tau}}\right)\left(\frac{\overline{1/\tau[\mathrm{OH}]}}{J_{\mathrm{ClONO2}}J_{\mathrm{NO2}}}\right)\left(\frac{[\mathrm{O_3}][\mathrm{Cl_y}]}{[\mathrm{CH_4}][\mathrm{NO_x}]}\right). \quad (14)$$

The ClO equations, (13) and (14), are revisited in the discussion. The remainder of our analysis focuses on gas-phase partitioning between $ClONO_2$ and HCl, and specifically on the ratio $[ClONO_2]/[HCl]$. The TASSP approximation, (12), provides a foundation for model-measurement comparisons, error propagation, and statistical treatment. This versatility establishes $[ClONO_2]/[HCl]$ as our primary metric of partitioning.

3.4. Steady State $[ClONO_2]/[HCl]$ During POLARIS

Figure 6 shows the approximately linear relationship between observed $[ClONO_2]/[HCl]$ and observed $[O_3]^2/[CH_4]$. Similar relations, based on remote observations, were demonstrated by *Dessler et al.* [1995] and *Sen et al.* [1999]. The linear relationship between $[ClONO_2]/[HCl]$ and $[O_3]^2/[CH_4]$ implies that the tracer term dominates (12) and therefore, to first order, controls inorganic chlorine partitioning. Figure 7 shows observed $[O_3]^2/[CH_4]$ and observed $[ClONO_2]/[HCl]$ as functions of pressure and latitude. Tables 4 and 5 summarize the $[ClONO_2]/[HCl]$ observations. Within the lower stratosphere, twenty-fold variations in $[O_3]^2/[CH_4]$ induce similar variations in $[ClONO_2]/[HCl]$.

Departure from the linear relationship between $[ClONO_2]/[HCl]$ and $[O_3]^2/[CH_4]$ (scatter in Figure 6) is caused largely by the secondary factors K and F. Using equation (12), both K and F can be calculated explicitly and compared with observations. For example, dividing observed $[ClONO_2]/[HCl]$ by $[O_3]^2/[CH_4]$, K calculated from JPL97, and the constant 0.91 provides an atmospheric determination of F. Figure 8a compares this "observed" F with its calculated counterpart (11) as a function of latitude. The similar latitude-dependence of the observed and calculated F demonstrates that the photolytic processes controlling inorganic chlorine partitioning are well characterized by the linear reaction set (reactions (R1)-(R8)). Figure 8b shows that the seasonal trends in F are also in agreement, but to a lesser degree. The absolute offset between the observed and calculated values in Figures 8a-8d reveals a fundamental discrepancy between the observations and the inorganic chlorine chemistry of JPL97. While the offset is large, it is within the ±90% 1σ limits determined by the uncertainties in the rate constants, photolysis rates, and observations.

A similar analysis (now using F from (11)) produces an atmospheric determination of K. This "observed" K is plotted along with K calculated directly from JPL97 as a function of pressure in Figure 8c. The similar pressure dependence of the observed and calculated K confirms the existence of (R2) as an association reaction driving gas-phase Cl_y partitioning. In Figure 8d, K is divided by P (to remove the pressure dependence) and plotted versus temperature. The temperature dependence of observed K/P is not consistent with the chemistry of JPL97: while calculated K/P is independent of temperature, observed K/P decreases linearly with temperature, dropping by approximately a third over the observed temperature range.

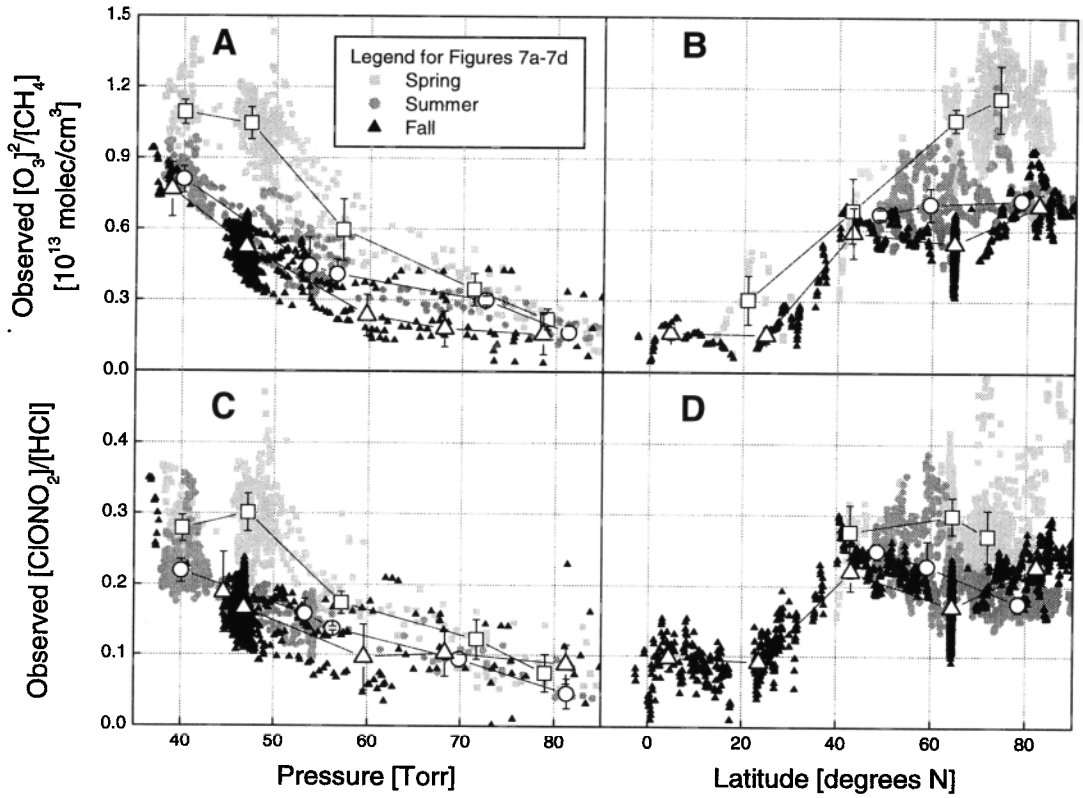

Figure 7. $[O_3]^2/[CH_4]$ as a function of (a) pressure and (b) latitude during the spring (April/May), summer (July/August), and fall (September). (c) and (d) Analogous plots for $[ClONO_2]/[HCl]$. The pressure dependence is restricted to 60°-70°N latitude, while the latitude dependence is restricted to (53-67 mbar). Bin medians and interquartile ranges are superimposed on the data.

Temperature, however, is strongly correlated with latitude in the POLARIS data set. Observed temperatures less than ~215 K in the lower stratosphere occur south of 40°N latitude, while temperatures greater than ~215 K occur north of this latitude. Temperature dependence can therefore appear as latitude dependence (Figure 8a) and as altitude dependence (Figure 8c). Removing the temperature dependence using data from Figure 8d generally improves the agreement between the observations and calculations in Figures 8a and 8b and has almost no effect on Figure 8c. These results suggest that the apparent temperature dependence in Figure 8d is real and is not the result of a latitude-dependent error in the photolysis rates. The absolute discrepancy between the observed and calculated variables (Figures 8a-8c) reflects the fact that 85% of the observations were made at temperatures greater that 215 K where the probable temperature-dependent error is greatest.

Similar results are found when using JPL00 rate constants. These recent revisions have the most pronounced effect on Figure 8d, decreasing calculated *K/P* by approximately 8% at 200 K, 5% at 220 K, and 4% at 230 K. This change exacerbates the temperature-dependent discrepancy in Figure 8d at the same time that it generally improves agreement in Figures 8a, 8b, and 8c; calculated values in all these plots are reduced by approximately 5%, with a somewhat greater decrease at low latitudes in Figure 8a.

The latitude and pressure dependence of the secondary factors (Figures 8a and 8c) counteracts that of $[O_3]^2/[CH_4]$ (Figure 7a and 7b) and therefore reduces the overall latitude and pressure dependence of $[ClONO_2]/[HCl]$ (Figures 7c and 7d). The influence of the secondary factors is most evident, however, along trajectories. During the advection of an air mass, K and F dominate (12) because $[O_3]^2/[CH_4]$ acts as a tracer and scales only with density owing to the long photochemical lifetime of O_3 and CH_4. For a midlatitude air parcel that is advected 30° north, $[ClONO_2]/[HCl]$ will be up to 50% greater than its local value because of the gradient in F (Figure 8a). Similar memory effects occur when air parcels are subject to altitude perturbations since higher pressures and lower temperatures increase both K and $[O_3^2]/[CH_4]$ (via mixing ratio effect) while lower J_{ClONO2} increases F. Seasonal memory effects will be negligible during the spring and summer because F changes little over the 10 day lifetime (Figure 8b).

In summary, the TASSP approximation provides a framework for understanding gas-phase inorganic chlorine partitioning in the lower stratosphere. This analysis reveals a model-measurement discrepancy that increases with temperature and exceeds 50% at 225 K. The more complete ARSNIP model is required to confirm, quantify, and localize this probable error.

4. Quantitative Analysis of Inorganic Chlorine Partitioning

4.1. Description of the ARSNIP Model

The Augmented Reaction Set Numerical Integration Partitioning (ARSNIP) model is designed to estimate

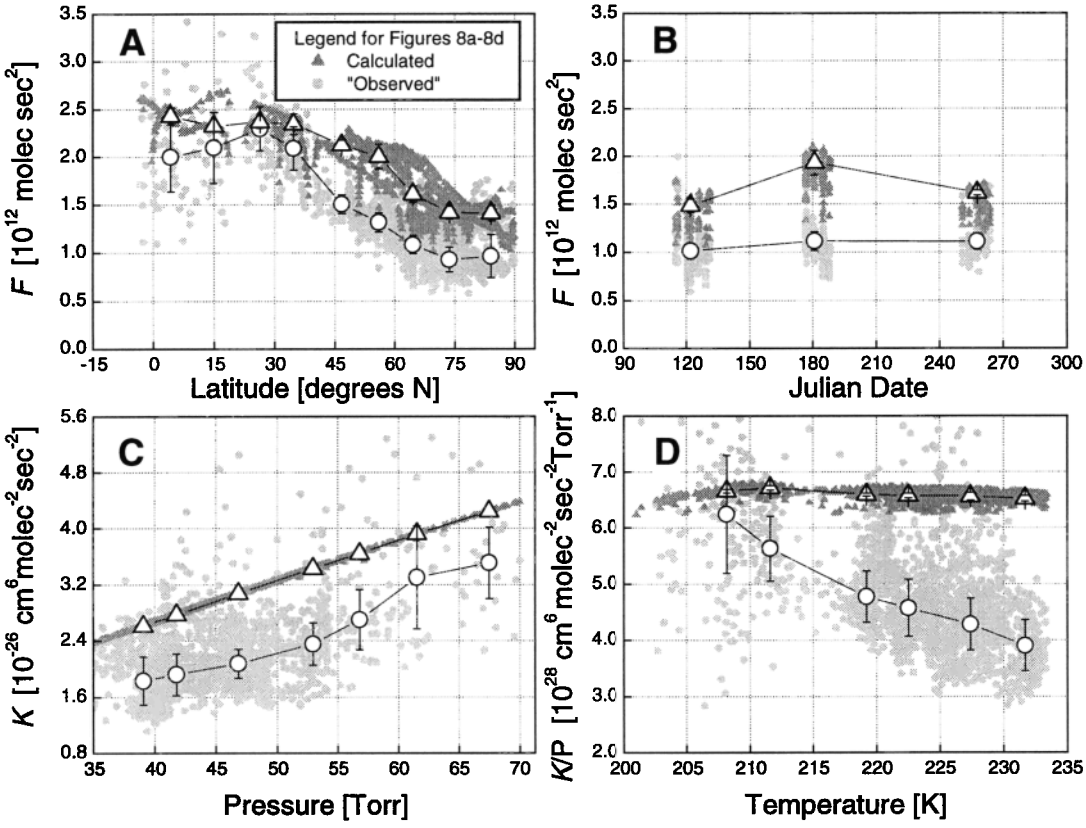

Figure 8. Secondary control of Cl_y partitioning by K and F in equation (12). Calculated and "observed" values show how $[ClONO_2]/[HCl]$ is influenced by (a) latitude, (b) season, (c) pressure and, unexpectedly, by (d) temperature. Data are restricted to P<93 mbar and in plot (b) only to 60°-70°N latitude. Bin medians and interquartile ranges (IQR) are superimposed on the data.

$[ClONO_2]/[HCl]$ in accordance with the complete gas-phase inorganic chlorine chemistry of JPL97 (minor changes introduced by JPL00 are discussed where appropriate). This model retains much of the simplicity of the TASSP approximation, but uses a more complete reaction set (reactions (R1)-(R19) from Table 1) to permit quantitative comparisons between simulated and observed $[ClONO_2]/[HCl]$.

Like the TASSP approximation, the ARSNIP model is constrained by [OH] observations parameterized as a function of SZA and pressure (1). The ARSNIP model is also simplified by setting $[NO_x]$ to its (constant) observed value while allowing NO and NO_2 to repartition. The constant-$[NO_x]$ assumption is supported by the absence of NO_x in the TASSP approximation (12) and by the modest diurnal variation in $[NO_x]$ observed during POLARIS [*Del Negro et al.*, 1999; *Perkins et al.*, 2001].

In the standard model run, reactions (R1)-(R19) were integrated for 30 days using a Backwards Euler/Newton-Raphson procedure with a 30-min time step [*Gotlub and Ortega*, 1992; *Press et al.*; 1988, *Gunther et al.*, 1973; S. C. Wofsy, personal communication, 1998]. The model was run at approximately 2-min intervals along the flight track using the time grid from the JPL PSS model (described in section 2.1). Model inputs included observed $[O_3]$, $[CH_4]$, and $[NO_x]$, $[C_2H_6]$ derived from $[N_2O]$, the approximate mission-average H_2 mixing ratio (0.5 ppmv), the [OH]-SZA parameterization, and calculated photolysis rates for the species $ClONO_2$, NO_2, O_3, and H_2CO. Depending on the particular model run, photolysis rates were based either on the local albedo or on the climatological average albedo (see section 2.2). All runs were initialized using $[ClONO_2]$, [HCl], [ClO], [Cl], [NO], $[NO_2]$, and $[H_2CO]$ from the JPL PSS model; the initialization, however, does not significantly effect simulated $[ClONO_2]/[HCl]$. Figure 2 shows a schematic diagram of the ARSNIP model. Sections 1 and 2 of this paper provide additional information on the model inputs and chemistry.

The [OH]-SZA parameterization and constant-$[NO_x]$ assumption were tested using sensitivity analysis. In the worst case, under extreme low-$[NO_x]$ conditions, a 50% change in $[NO_x]$ induced a only a 3% change in modeled $[ClONO_2]/[HCl]$. Other tests confirmed that $[ClONO_2]/[HCl]$ is insensitive to realistic variations in the amplitude and phase of the diurnal $[NO_x]$ cycle. Thus no data points were removed from the analysis due to sensitivity to $[NO_x]$. Sensitivity to the [OH]-SZA parameterization was tested by changing the zero intercept of the parameterization from 94.5° to 93° and examining the resulting change in $[ClONO_2]/[HCl]$. Approximately 130 out of a possible 2340 model runs were removed because $[ClONO_2]/[HCl]$ changed by more than 4% for a 1.5° change in the zero intercept.

Model runs were also removed if the lifetime for Cl_y partitioning exceeded 15 days, if the ER-2 intercepted an aircraft exhaust plume, or if observations of critical species were absent within the interval ±60 s about the modeled point. Most

Table 4. Observed $[ClONO_2]/[HCl]$ (Bin Medians ± IQR/2) Versus Pressure at 60°-70°N

Deployment	47-60 mbar	60-73 mbar	73-87 mbar	87-100 mbar	100-113 mbar
Spring	0.28 ± 0.02	0.30 ± 0.03	0.17 ± 0.02	0.12 ± 0.03	0.08 ± 0.03
Summer	0.22 ± 0.02	0.16 ± 0.02	0.14 ± 0.03	0.09 ± 0.01	0.05 ± 0.02
Fall	0.19 ± 0.06	0.17 ± 0.02	0.10 ± 0.05	0.10 ± 0.03	0.09 ± 0.03

of the eliminated runs were from high-latitude flights during September. In total, 1543 runs of the fixed-latitude ARSNIP model met the necessary criteria for inclusion in the analysis.

For trajectory runs the ARSNIP model was driven by 10-day histories of temperature, pressure, latitude, and longitude for each modeled point along the flight path. Trajectory information was provided by the Goddard Space Flight Center (GSFC) isentropic trajectory model [*Schubert et al.*, 1993]. Since $[ClONO_2]/[HCl]$ is much more sensitive to albedo than overhead ozone (see discussion of equation (11)), the trajectory runs included albedo information while holding overhead ozone to its flight-intercept value. Albedo was allowed to change along the back trajectories according to the same lookup table (zonal average TOMS reflectivity versus latitude and deployment) used for the fixed-latitude model. Trajectory runs also used the same time grid as the fixed-latitude model with each run driven by the trajectory nearest in time along the flight track (always less than ~2.5 min away). In total, 1360 runs of the trajectory ARSNIP model met the criteria for inclusion in the analysis.

Trajectory runs were initialized to the same conditions as the fix-latitude runs. Each trajectory run, however, was iterated four times with the output of successive iterations serving as input to the next. By the final iteration this scheme essentially initializes each trajectory to its average value of temperature, pressure, latitude, and species concentration. For comparison with fixed-latitude models, this initialization is more conservative than those based on uncertain conditions at the beginning of the trajectories.

The simplicity of the ARSNIP model in both its fixed-latitude and trajectory form permitted extensive validation and experimentation. These tests included variations in the [OH]-SZA parameterization, back trajectories, photolysis rate calculations, model initialization, and numerical methods, as well as changes in the modeled reactions and rate constants.

4.2. Comparison of Modeled and Observed $[ClONO_2]/[HCl]$

Results from four runs of the ARSNIP model are compared with observations in Figure 9. As discussed below, the general trend of improving precision (decreasing scatter) and increasing overestimation of $[ClONO_2]/[HCl]$ in the four plots (Figures 9a-9d) parallels improvements in the model assumptions and photochemistry.

In all of the plots in Figure 9, regression lines are calculated using midlatitude and polar data (latitude>40°N and T≈225 K). The flight of April 26, 1997, is treated separately because rapid northward advection of the sampled air mass perturbed its Cl_y chemistry. Regressions are calculated using log-transformed data in order to assure that they are independent of the ratio definition (i.e., $[ClONO_2]/[HCl]$ or $[HCl]/[ClONO_2]$) and unbiased by variance that increases with the mean. All regressions are constrained to pass through the origin. The uncertainty limits for the regressions are estimated by error propagation (using Table 3 and equation (12)). The precision limits, which are calculated directly from the model-measurement regressions, are negligible in comparison. The model and observations are considered in agreement when the uncertainty limits overlap the 1:1 line. Table 6 summarizes the regression statistics of six model runs, including the four plotted in Figure 9. These summary statistics consist of the slope (systematic error in the model with respect to observations) and the coefficient of determination (R^2 ranges from zero for complete scatter to one for a perfect linear relationship).

Figure 9a shows the results of a model verification run. In this test, the ARSNIP model simulates the complete photochemistry of JPL97 as implemented in the JPL PSS model constrained by observed NO_y. This test is accomplished by driving the ARSNIP model with an [OH]-SZA parameterization that is based on the output of the JPL PSS model. Because the [OH]-SZA relation is not as tight in the JPL PSS model as it is in the atmosphere, a separate relation for each point along the flight track is constrained to pass through the zero intercept, [OH]=0 at SZA=94°, and the [OH]-SZA pair estimated by the JPL PSS model for that flight point. To prevent large extrapolation errors in estimated [OH], flight points with SZA>80° are not modeled. Individual [OH]-SZA relations for each flight point are used only during the verification of the ARSNIP model (Figure 9a and row 2 of Table 6).

In this verification mode the ARSNIP model always estimates $[ClONO_2]/[HCl]$ within approximately ±20% of the corresponding JPL PSS simulation. More detailed tests reveal that the point by point differences between the two models are due largely to their differing treatments of [OH]; the [OH]-SZA parameterization used in the ARSNIP model only roughly approximates the diurnal cycle of [OH] in the JPL PSS model. Furthermore, when the JPL PSS model's [OH] is too high relative equation (1), its $[ClONO_2]/[HCl]$ is too high relative to the ARSNIP model. Averaged over all of POLARIS, the ARSNIP model and JPL PSS model are in excellent agreement (compare rows 1-2, Table 6). The greater scatter (lower R^2) in the output of the JPL PSS model demon-

Table 5. Observed $[ClONO_2]/[HCl]$ (Bin Medians ± IQR/2) Versus Latitude at 53-67 mbar

Deployment	-10°-10°N	10°-30°N	30°-50°N	50°-70°N	70°-90°N
Spring	-	-	0.28 ± 0.04	0.30 ± 0.03	0.27 ± 0.04
Summer	-	-	0.25 ± 0.01	0.23 ± 0.04	0.18 ± 0.01
Fall	0.10 ± 0.02	0.09 ± 0.02	0.22 ± 0.03	0.17 ± 0.02	0.23 ± 0.02

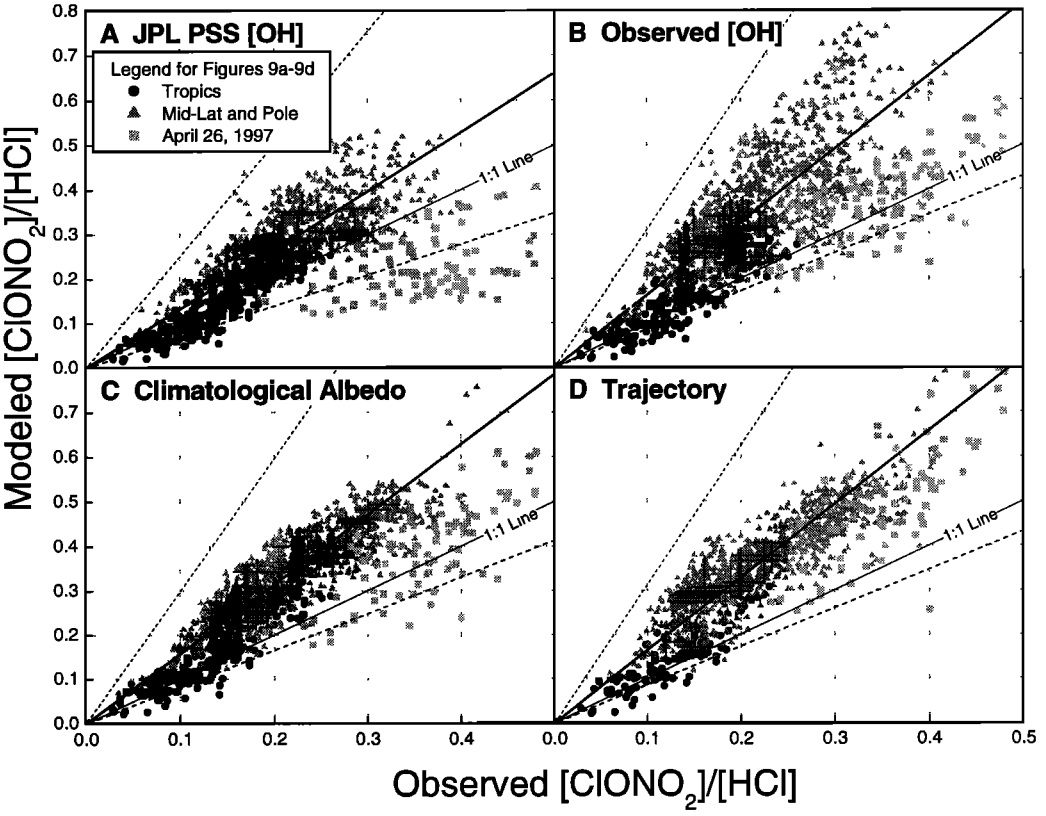

Figure 9. Results from the ARSNIP model for P<93 mbar. In all plots, modeled [$ClONO_2$]/[HCl] is regressed against its observed value. Symbols designate the tropics (latitude<40°N, T<215 K) and the midlatitude and polar regions (latitude>40°N, T >215 K). The air mass encountered during the flight of April 26 retains a signature of low-latitude solar exposure. The expected 1:1 relationship (thin solid line), best fit to the midlatitude and polar data (thick solid line), and 1σ error limits (dashed lines) are shown for reference. Details of the four model versions are provided in the text.

strates that JPL97 HO_x photochemistry is a significant source of noise when modeling inorganic chlorine partitioning.

In Figure 9b the ARSNIP model is identical to the verification run except that the [OH]-SZA parameterization is constrained by observations rather than the output of the JPL PSS model. In the midlatitude and polar regions (~85% of the POLARIS data), the [OH] constraint exposes an additional ~23% error in modeled partitioning but does not effect the scatter (compare slopes in rows 2-3, Midlatitude/Pole column of Table 6). This result is consistent with the known (roughly) 18% underestimate of observed [OH] by the JPL PSS model at moderate to large solar zenith angles [*Wennberg et al.*, 1999]. The difference in the [OH] and [$ClONO_2$]/[HCl] errors (compare 18% with 23%) is due to biases in the OH-parameterization (e.g., the function cannot represent [OH] equally well over all SZA and at all latitudes as evident in Figure 3b).

Recent updates in the rate constants for the reactions $OH+NO_2$ [*Dransfield et al.*, 1999] and $OH+HNO_3$ [*Brown et al.*, 1999] as implemented by *Gao et al.* [1999], *Osterman et al.* [1999], and *Wennberg et al.* [1999] reduce scatter in the output of the JPL PSS model and bring it into better agreement with the ARSNIP model (compare rows 1,3, and 6, Midlatitude/Pole column in Table 6). Even with these improvements, however, the JPL PSS model on average underestimates observed [OH] by (roughly) 10% and therefore underestimates [$ClONO_2$]/[HCl] by a similar amount (15%) in comparison with the ARSNIP model. Again, the OH parameterization appears to introduce a modest bias. Implementing the complete JPL00 chemistry for the JPL PSS model

Table 6. Slope and Coefficient of Determination for Model-Measurement Regressions

Model Description	Tropics (<40°N)		Midlatitude/Pole (>40°N)		April 26 Flight	
	Slope	R^2	Slope	R^2	Slope	R^2
1. JPL PSS (JPL97, NO_y constrained)	0.92	0.79	1.31	0.41	0.56	0.16
2. ARSNIP (JPL PSS [OH])	0.92	0.78	1.32	0.60	0.62	0.13
3. ARSNIP (observed [OH])	1.04	0.76	1.63	0.61	1.05	0.57
4. ARSNIP (average albedo)	1.09	0.78	1.57	0.78	1.06	0.52
5. ARSNIP (10-day trajectory)	1.08	0.68	1.65	0.67	1.38	0.54
6. JPL PSS (new NO_y and HO_x chemistry)	0.96	0.77	1.40	0.62	0.74	0.17

is beyond the scope of this paper; changes, however, are likely to be small. On the basis of our TASSP model and consideration of the significant increase in the recommendation for k_{ClO+OH}, we expect the new rates to decrease simulated $[ClONO_2]/[HCl]$ by less than 10% in the ARSNIP and JPL PSS models.

The version of the ARSNIP model in Figure 9c is identical to that in Figure 9b, except that the photolysis rate calculations are based on climatological average albedo rather than the local albedo measured beneath the ER-2. By eliminating the transient effect of clouds, these climatological average photolysis rates improve model estimates of long-lived species that are sensitive to albedo. When using climatological photolysis rates, the ARSNIP model estimates $[ClONO_2]/[HCl]$ with substantially greater precision than it does when using local photolysis rates (compare R^2 in rows 3-4, middle column of Table 6). A modest change in the slope (the overestimate of $[ClONO_2]/[HCl]$ drops from 1.63 to 1.57) indicates that, on average, the albedo measured along the ER-2 flight track differs somewhat from the TOMS climatological mean.

Figure 9d shows the output from the trajectory version of the ARSNIP model. This model run explains much of the anomalous partitioning observed during the flight of April 26, 1997. The air mass sampled during this flight was unusual in that it moved north by 30°-40° during the few days prior to flight intercept. Since northward advection is equivalent to translation down the F gradient of the TASSP approximation (see equation (12) and Figure 8a), the air mass retains a signature of its low-latitude solar exposure. All of the fixed-latitude models therefore underestimate $[ClONO_2]/[HCl]$ for this flight.

Unexpectedly, the trajectory simulation significantly increases the scatter of the model-measurement regression relative to the same regression generated by the fixed-latitude version of the ARSNIP model (compare R^2 in rows 4-5, Tropics and Midlatitude/Pole columns of Table 6). Partial trajectories that hold latitude or altitude constant reveal that both these parameters are equally responsible for the introduced scatter. Furthermore, the scatter decreases as the trajectory is shortened, approaching that of the fixed-latitude model for a 1-day trajectory. Since the fixed-latitude and trajectory versions of the ARSNIP model use the same inputs and chemistry, the lower precision of the trajectory version may imply that, from late spring through early fall, the GSFC trajectories are less representative of the real motion of the atmosphere than the zero-order assumption of fixed latitude.

The trajectory version of the ARSNIP model does, however, account for geographical constraints. As expected, allowing for trajectory history has the greatest effect on high-latitude simulations. At high northern latitudes most air parcels arrive from the south, and trajectory model estimates of $[ClONO_2]/[HCl]$ exceed fixed-latitude estimates due to the latitude gradient in F. At the North Pole, for example, all air parcels arrive from the south and $[ClONO_2]/[HCl]$ estimated by trajectory models will always exceed the ratio estimated by fixed-latitude models. At mid to high latitudes, allowing for trajectory history increases the overestimate of $[ClONO_2]/[HCl]$ by approximately 5% on average.

In consideration of the possible bias in the OH-parameterization (which is similar in magnitude and direction to the trajectory effect), we conservatively select the non-trajectory, climatological albedo model as the most accurate and precise implementation of JPL97 (reactions (R1)-(R19)). This model overestimates observed $[ClONO_2]/[HCl]$ in the midlatitude and polar regions (T≈225 K) by approximately 57% (henceforth 55-60%). In the tropics (T≈210 K), modeled $[ClONO_2]/[HCl]$ exceeds the observed value by approximately 10%. JPL00 rate constants decrease these overestimates by almost 10% but do not otherwise change our conclusions.

4.3. Localizing Errors in Inorganic Chlorine Partitioning

Examination of the inorganic chlorine budget [*Bonne et al.*, 2000] and $[ClO]/[ClONO_2]$ [*Stimpfle et al.*, 1999] provides additional insight into the model-measurement discrepancy in $[ClONO_2]/[HCl]$. The budget reveals differences between inferred $[Cl_y]$ and the sum of its primary constituents (observed [HCl], $[ClONO_2]$, and [ClO]). Note that $[Cl_y]$ is estimated independently as total chlorine entering the stratosphere minus the (primarily) observed in situ halocarbon concentration. Because the budget analysis does not rely on rate constants or photolysis rates, it provides an assessment of potential errors in the species measurements. Examination of $[ClO]/[ClONO_2]$, in contrast, checks a subset of the rate constants, photolysis rates, and measured species in (R1)-(R19).

Model-measurement discrepancies for all three inorganic chlorine studies are plotted as percent error versus temperature in Figure 10. In Figure 10a, error is defined as the percentage by which inferred $[Cl_y]$ exceeds the sum of measured [HCl], $[ClONO_2]$, and [ClO]. In Figures 10b and 10c, error is defined as the percentage by which model estimates exceed the observations of $[ClONO_2]/[HCl]$ and $[ClONO_2]/[ClO]$, respectively. $[ClONO_2]/[HCl]$ is estimated by the climatological albedo version of the ARSNIP model (row 4 of Table 6), and $[ClO]/[ClONO_2]$ is calculated using the dynamic steady state approximation (equations (6)-(8)). While the plots exhibit considerable scatter, the standard regression lines are well determined as shown by their 95% confidence limits (precision error only). Bin medians and interquartile ranges support the temperature dependence but suggest a flattening of the regressions at temperatures above 215 K.

Because temperature and latitude are strongly correlated, the effects of these two variables on the model-measurement discrepancies are first examined separately. Table 7 lists the least squares slopes and 95% confidence intervals for the three studies in Figure 10. The first column in the table summarizes the temperature dependence for the entire data set, the second column shows temperature dependence within a narrow latitude bin (70°-80°N) and the third column shows latitude dependence within a narrow temperature bin (218-223 K). In all three studies the temperature dependence is nearly unchanged by the latitude constraint (compare columns 1 and 2) and eliminated by the temperature constraint (compare columns 1 and 3, noting that temperature and latitude are positively correlated). The constrained regressions therefore imply that temperature, rather than latitude, drives model-measurement discrepancies in Figure 10.

Figure 10a shows that the error in the budget grows to approximately 15% at the lower end of the observed temperature range (205 K). This low-temperature discrepancy can be attributed largely to errors in inferred $[Cl_y]$ or measured [HCl], or to an unmeasured chlorine species that becomes more prevalent at low temperature; $ClONO_2$ makes up too

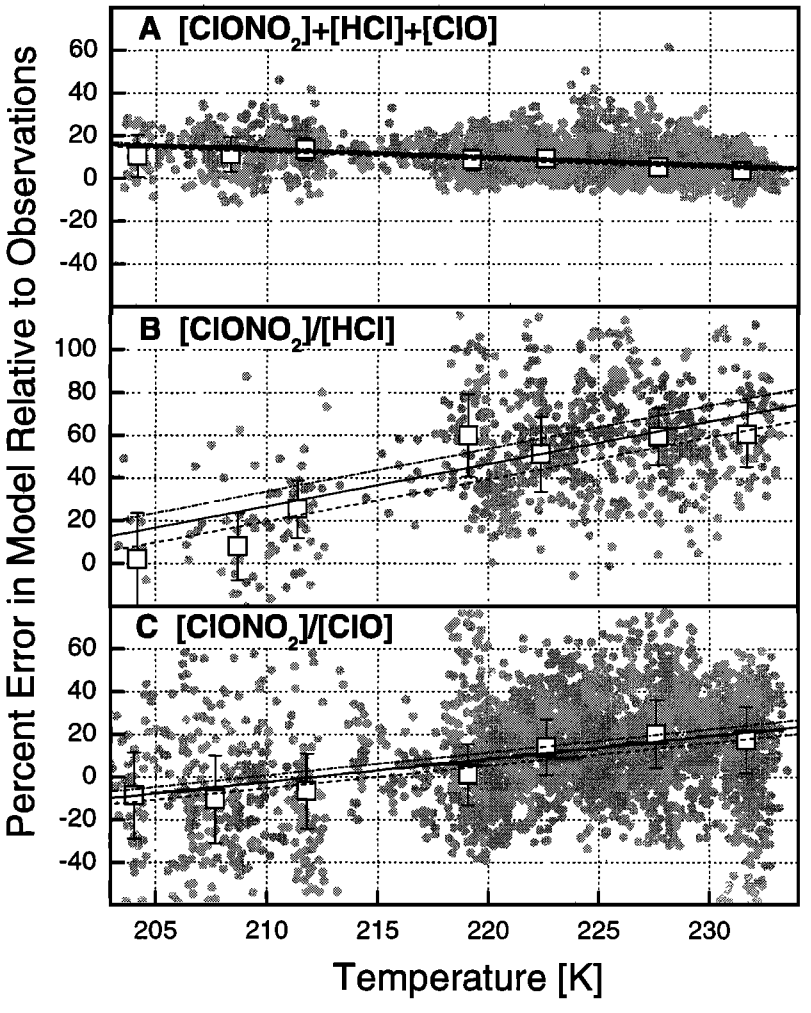

Figure 10. Temperature dependence of the model-measurement discrepancy in three studies of POLARIS inorganic chlorine. All plots show percent error in the model relative to observations, bin medians (squares) and interquartile ranges, a least squares fit (solid line), and its 95% confidence interval based on precision only (dashed lines). (a) The budget is inferred [Cl_y] divided by observed [HCl]+[$ClONO_2$]+[ClO] and converted to percent. Model/measurement percentage error is shown for the quantities (b) [$ClONO_2$]/[HCl] and (c) [$ClONO_2$]/[ClO]. All data are restricted to P<93 mbar and exclude observations made during rapid changes in aircraft altitude (e.g., dives). Extreme outliers (more than 5 times or less than 1/5 of the mean) are removed, and a few additional data points are cropped by the graph axes. In Figure 10c the data are further restricted to SZA<85°, and outliers beyond the 95th percentile are removed using a median filter.

small a fraction of Cl_y to induce a 15% error in the budget. *Bonne et al.* [2000] show that a constant mixing ratio offset error of approximately 110 ppt in either Cl_y (measurement too high) or HCl (measurement too low) can explain the error in the budget over the observed temperature range. An alternative suggestion that some HCl is sequestered in liquid aerosols and therefore not measured at low temperatures (*D. J. Jacob,* personal communication, 1998) does not appear to be consistent with the observations; at a fixed temperature, higher aerosol surface area is correlated (weakly) with lower error in the budget.

Table 7. Slopes and 95% Confidence (x10^3) From Figure 10

Study	All POLARIS	70<LAT<80 (218<T<234)	218<T<223 (45<Lat<90)
Budget	3.0 ± 0.3	6.6 ± 0.9	0.3 ± 0.3
[$ClONO_2$]/[HCl]	-13.1 ± 1.6	-12.0 ± 3.3	1.7 ± 1.3
[$ClONO_2$]/[ClO]	-10.9 ± 1.3	-8.5 ± 3.0	1.6 ± 1.1

The temperature dependence in the [$ClONO_2$]/[HCl] study (~1.4%/K; Figure 10b) is consistent with, but larger than, any hypothetical HCl measurement error suggested by the temperature dependence in the budget (~0.3%/K). A reduction in the temperature dependence of k_{NO+O3} [*Del Negro et al.,* 1999; *Cohen et al.,* 2000] is also consistent with the [$ClONO_2$]/[HCl] study, explaining ~0.5%/K. The remaining (unexplained) temperature dependence in the [$ClONO_2$]/[HCl] study (~0.6-0.9%/K) can be localized within [$ClONO_2$]/[ClO] (1.0%/K; Figure 10c) and, most likely, within one or more of the variables common to both partitioning studies (J_{ClONO2}, $k_{ClO+NO2}$, and observed [$ClONO_2$]). The temperature dependence should be interpreted with caution, however, since it is largely driven by the four flights that sampled the tropical stratosphere (April 22 and September 21,

23, and 25 of 1997). The JPL00 rates augment the temperature-dependence of the discrepancy in $[ClONO_2]/[HCl]$ by less than 10% and therefore do not appreciably change our conclusions.

More significant is the model-measurement discrepancy in $[ClONO_2]/[HCl]$ at 225 K (Figure 10b). At this temperature, which represents the majority of the observations, modeled $[ClONO_2]/[HCl]$ is approximately 55-60% higher than the observed ratio (consistent with Figures 8 and 9 and Table 6). This discrepancy is not substantially changed by any of the probable budget errors discussed above. Furthermore, it is unlikely that the HCl measurement is a significant source of error; correcting [HCl] to force partitioning agreement upsets the chlorine budget. In fact, errors in the budget and partitioning are opposite in sign if they are attributed to [HCl].

All three studies in Figure 10, however, are consistent with a systematic error in the $ClONO_2$ measurement (possibly too low). For example, a 20% increase in observed $[ClONO_2]$ decreases the budget error at 225 K from 7% to 4%, reduces the discrepancy in $[ClONO_2]/[HCl]$ from 55-60% to 29-33%, and shrinks the overestimate of $[ClONO_2]/[ClO]$ from 17% to -2% (note that errors are multiplicative: 1.60/1.20=1.33). The presence of a common error in the ClO and $ClONO_2$ calibrations would allow the error in $ClONO_2$ to exceed 20% without exacerbating the model-measurement discrepancy in $[ClONO_2]/[ClO]$ (i.e., reducing it below -2%).

Adding to this indirect evidence, *Toon et al.* [1999] show that the ER-2 observations of $[ClONO_2]$ during the first POLARIS deployment are approximately 30% lower than the corresponding MarkIV (balloon) observations at the same altitude. The intercomparison is based on altitude (rather than N_2O) because the ER-2 and MarkIV measurements of both $[O_3]$ and $[CH_4]$ agree on average within 2% in this reference frame and, furthermore, because the lifetime of Cl_y partitioning is less than 10 days (i.e., partitioning does not act as a tracer). Excellent agreement between the ER-2 and MarkIV observations for 17 other species (always within 20% and usually within 10%) provides additional confidence in the intercomparison; the 30% disparity in $ClONO_2$ is an anomaly. *Sen et al.* [1999] find somewhat better agreement between the MarkIV and ER-2 $ClONO_2$ observations, but their intercomparison is based on the ER-2 flight of April 26, 1997 which had unusually high $[ClONO_2]/[HCl]$ (see discussion of Figure 9d in section 4.2).

If the ER-2 $ClONO_2$ observations are in fact 20-30% low, then the corrected $[ClONO_2]/[ClO]$ observations are in good agreement with models (within ~10%) and the remaining model-measurement discrepancy in $[ClONO_2]/[HCl]$ (20-35%) is most directly attributed to the measured species, rate constants, and reactions that link HCl and ClO. As discussed above, JPL00 rate constants decrease this model-measurement discrepancy by nearly 10%, but do not appreciably change our conclusions.

Modeled production of HCl may be too slow (due to missing chemistry, low measurements of [NO] or $[CH_4]$, or low JPL97 rates for the reactions (R3), (R5), (R9)-(R12)). Alternatively, modeled loss of HCl may be too fast (either (R4), (R6), [OH] or $[O_3]$ is too high). An analysis of POLARIS NO_x partitioning [*Del Negro et al.*, 1999] suggests that $k_{NO+O3}[NO]$ may be too low (not too high as suggested above). It is therefore unlikely that (R3) or measured [NO] are significant sources of error in Cl_y partitioning. Redundancy in the ER-2 measurements of $[CH_4]$ and good agreement between the ER-2 and MarkIV observations of both $[CH_4]$ and $[O_3]$ [*Toon et al.*, 1999] eliminate the tracer measurements as probable causes for the model-measurement discrepancy in $[ClONO_2]/[HCl]$.

Previous studies provide some insight into possible rate constant errors. *Michelsen et al.* [1996], for example, propose a weighted fit to reported rate data that increases k_{Cl+CH4} by approximately 30% in comparison with the JPL97 recommendation at temperatures near 215 K (25% in comparison with the JPL00 recommendation). This change improves model agreement with the ATMOS data and reduces the ARSNIP model overestimation of $[ClONO_2]/[HCl]$ by 17%. Recent laboratory measurements of k_{Cl+OH} [*Kegley-Owen et al.*, 1999] reduce the ARSNIP model overestimation by 3%, while new values of k_{HCl+OH} [*Battin-Leclerc et al.*, 1999] increase it by 8%. The uncertainty in many of these rate constants, however, is large at low temperatures. Measured rates for the reaction $Cl+O_3$, for example, can exceed the JPL97 recommendation by more than 20% at 220 K [*Nicovich et al.*, 1990], potentially offsetting the change in k_{Cl+CH4} proposed by *Michelsen et al.* [1996]. In fact, competitive chlorination studies appear to constrain k_{Cl+O3}/k_{Cl+CH4} (the relevant quantity for Cl_y partitioning in (12)) to within approximately 15% [*DeMore*, 1991], leaving k_{OH+HCl}, observed [OH], and missing chemistry as the most probable sources of error in Cl_y partitioning.

Direct observation of the $ClONO_2$-HCl lifetime would be particularly useful for distinguishing between these scenarios. The predicted lifetime will decrease if k_{Cl+CH4}, k_{Cl+O3}, k_{ClO+NO}, or missing HCl-production chemistry is responsible for the error in Cl_y partitioning. In contrast, correcting k_{OH+HCl} or observed [OH] will result in a lifetime that is 70% longer. While the diurnal variation in $[ClONO_2]/[HCl]$ is too small to discriminate between these two lifetimes (except possibility in the lower tropics), a time series of observations following a PSC (polar stratospheric cloud) processing event may constrain the probable source of error.

In summary, studies of the inorganic chlorine budget, $[ClONO_2]/[HCl]$, and $[ClONO_2]/[ClO]$, as well as an intercomparison of ER-2 and MarkIV observations, are all consistent with substantial errors in the rate constants linking HCl and ClO (modeled $[HCl]/[ClO]$ may be 20-35% too high) and, additionally, with a systematic error in the $ClONO_2$ measurement (possibly 20-30% too low). These conclusions hold for both the JPL97 and JPL00 reaction sets, but the discrepancy attributed to the rate constants is reduced to approximately 10-25% in the later case. Attribution of error to specific measurements and rate constants, however, is not absolute; more complex explanations for the various discrepancies must always be considered.

5. Discussion

In this section we briefly examine differences between the ARSNIP model and the JPL PSS model. With a better understanding of these differences, we reconcile our findings with previous studies of inorganic chlorine partitioning. Finally, we show how model simulations of [ClO] will be affected by our results and by changing stratospheric conditions.

Figure 11 shows that the ARSNIP model overestimates observed $[ClONO_2]/[HCl]$ by approximately 57% while the JPL

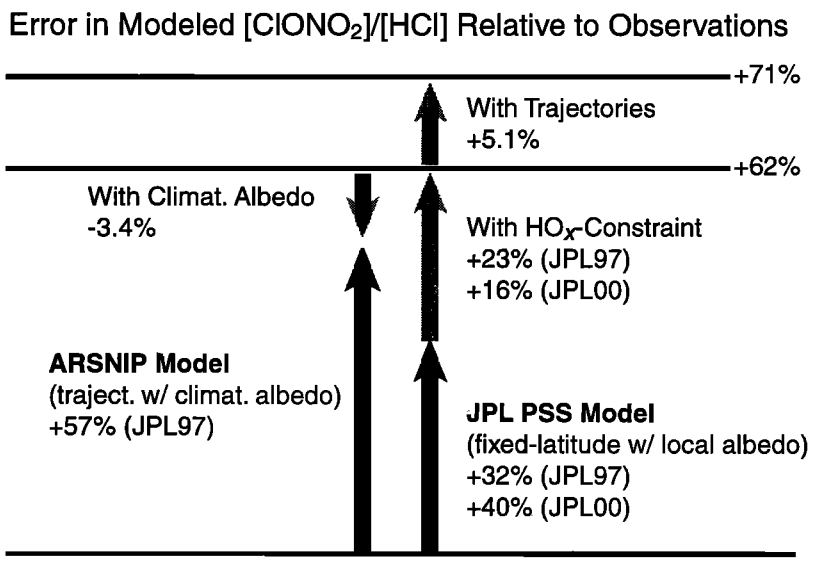

Figure 11. Errors in estimated $[ClONO_2]/[HCl]$ for the ARSNIP and JPL PSS models. Error (shown with black arrows) is defined relative to observed $[ClONO_2]/[HCl]$. Gray arrows show the effects of differing inputs and demonstrate that the two models are consistent with each other. Note that all errors are multiplicative (e.g., 1.32 x 1.23 = 1.62). The JPL97 reaction set includes the 6% production of HCl from the reaction ClO+OH [*Lipson et al.*, 1997]. Rates99 updates the rate coefficients k_{OH+NO2} [*Dransfield et al.*, 1999] and $k_{OH+HNO3}$ [*Brown et al.*, 1999].

PSS model overestimates this quantity only 32-40%. The difference between these two models is due to their divergent treatments of [OH] (parameterized versus modeled), albedo (climatological average versus local), and air parcel advection (trajectory versus fixed-latitude). As discussed above, we assert that the climatological albedo ARSNIP model (run 4 in Table 6) is the most realistic implementation of JPL97. Using JPL00 rates for the ARSNIP inorganic chlorine chemistry would reduce simulated $[ClONO_2]/[HCl]$ by less than 10%; the new rates, however, are not appropriate for the comparison in Figure 11 as the JPL PSS model used in our analysis is driven by JPL97 chlorine chemistry.

Our results appear to depart from earlier studies which generally show that models underestimate observed $[ClONO_2]/[HCl]$. During the Stratospheric Photochemistry and Dynamics Expedition (SPADE), for example, [HCl] measured by the ALIAS instrument onboard the ER-2 was approximately half the modeled value [*Webster et al.*, 1993, 1994a; *Salawitch et al.*, 1994a]. According to *Dessler et al.* [1995, p. 1724], the discrepancy between modeled and observed [HCl] from the Upper Atmosphere Research Satellite (UARS) "is similar in sign, but smaller in magnitude than seen in the (pre-POLARIS) ER-2 data." In contrast, and in better agreement with the present analysis, *Michelsen et al.* [1996] conclude that models slightly overestimate ATMOS (shuttle) observations of $[ClONO_2]/[HCl]$. Balloon-based [HCl] and $[ClONO_2]$ measurements in the lower stratosphere are generally in good agreement with modeled Cl_y partitioning [*Payan et al.*, 1998; *Sen et al.*, 1999].

Modeling differences explain some of the divergence in these conclusions. The ARSNIP model used in the present analysis is based on observed [OH], while all of the earlier analyses depend on simulated HO_x chemistry. If the POLARIS [OH] measurements are accurate, then an error in simulated HO_x chemistry may have diminished $[ClONO_2]/[HCl]$ in the previous models as it does in the present case. The previous models are also based on the assumption of fixed-latitude, further reducing their estimates of $[ClONO_2]/[HCl]$ and improving their agreement with observations.

If the ER-2 $ClONO_2$ measurement is systematically 20-30% low (as discussed in section 4.3), this would explain much of the remaining difference between the present analysis and remote observation studies (satellite, balloon, and shuttle measurements). The previous ER-2 study, in contrast, is not easily reconciled with the present analysis; however, interpretation of the earlier ER-2 data is complicated by the lack of a $ClONO_2$ measurement, missing inorganic chlorine in the budget, and a 6-year trend (increasing) in observed [HCl] [*Webster et al.*, 1998; *Bonne et al.*, 2000]. We therefore conclude that our results can be reconciled with most previous studies of inorganic chlorine partitioning in the lower stratosphere.

How do the findings of the present study effect models of the lower stratosphere in general? Correcting the probable errors in the rate constants linking HCl and ClO (increasing simulated [HCl]/[ClO] by ~25-30% as argued in section 4.3) will reduce estimates of [ClO] by approximately 5-10% (note that HCl and $ClONO_2$ constitute roughly 80% and 20% of Cl_y respectively). A decrease in modeled [ClO] of this magnitude would compound the effect of the recent revisions in the rate constants for $OH+NO_2$ [*Dransfield et al.*, 1999] and $OH+HNO_3$ [*Brown et al.*, 1999] which lower by several kilometers the altitude above which NO_x is predicted to dominate ozone loss [*Portmann et al.*, 1999]. In models this shift toward NO_x control reduces the predicted capacity of inorganic chlorine to buffer aircraft inputs of reactive nitrogen in the lower stratosphere [*Salawitch et al.*, 1994a; *Wennberg et al.*, 1994a; *Nevison et al.*, 1999].

Independent of any changes in the rate constants, we ex-

pect the role of chlorine in gas-phase ozone destruction to decline in the near term. As evident from the steady state approximation for [ClO] (equation (14)) anticipated trends in $[CH_4]\uparrow$, $[NO_x]\uparrow$, $[O_3]\downarrow$, $[Cl_y]\downarrow$, and temperature $\downarrow$ all tend to decrease [ClO]. While the magnitudes (and in some cases the signs) of these trends are uncertain, annual changes on the order of a fraction of a percent in the independent variables could act in concert (as a product in equation (14)) to reduce [ClO] in the summer lower stratosphere by 5-15% over the next decade.

The effects of rate constant errors and changing stratospheric composition are more difficult to generalize when applied to heterogeneous processes. The amount of ozone destroyed following heterogeneous conversion of HCl and $ClONO_2$ into reactive chlorine depends inversely on the length of the recovery as well as the specifics of the catalytic cycles that destroy ozone. The corrections shown in Figure 11 will tend to decrease the modeled recovery time (reducing ozone loss) by shifting steady state Cl_y partitioning further toward HCl and by shortening the partitioning lifetime. The recovery, however, is not controlled by chlorine chemistry alone; HNO_3 photolysis [*Liu et al.*, 1992], denitrification, and ozone depletion can profoundly effect the process. Furthermore, moderate changes in Cl_y partitioning will not change the outcome when ozone is lost completely as it is in some regions of the Antarctic. Because of these complexities, understanding the consequences of the present work for polar ozone loss is beyond the scope of this paper.

6. Conclusions

The POLARIS campaign produced the first in situ measurements of $[ClONO_2]$ and the most extensive set of direct observations describing gas-phase inorganic chlorine partitioning in the lower stratosphere. The lifetime for $ClONO_2$-HCl partitioning, 5-15 days during the spring and summer, supports the use of fixed-latitude and trajectory models in our analysis. Using accurate time constants, we develop an approximation for $[ClONO_2]/[HCl]$ (TASSP) that shows how solar exposure, pressure, temperature, and $[O_3]^2/[CH_4]$ control gas-phase inorganic chlorine partitioning in the lower stratosphere.

A more complete model (ARSNIP) demonstrates that the inorganic chlorine chemistry of JPL97 overestimates observed $[ClONO_2]/[HCl]$ by approximately 55-60% at mid and high latitudes ($T\approx225$ K) and that JPL00 rates reduce this discrepancy by less than 10%. A significant portion of this error may be attributed to the reactions, rate constants, and/or observed species concentrations that determine [ClO]/[HCl] (too high) as well as a possible systematic error in the ER-2 $ClONO_2$ measurement (too low).

We also find that climatological average photolysis rates (rather than local rates) significantly reduce scatter in comparisons of our ARSNIP model with observed $[ClONO_2]/[HCl]$. The climatological average ARSNIP model simulates the observations with even greater precision than an equivalent back trajectory model, implying that the summertime trajectories may be less accurate than the zero-order assumption of fixed latitude.

The substantial model-measurement discrepancy that we find in $[ClONO_2]/[HCl]$ is unusual, but not completely unexpected; models that include HO_x chemistry tend to agree better with observations because errors in their simulation of $[NO_x]$ and [OH] reduce their overestimate of $[ClONO_2]/[HCl]$ from 55-60% to approximately 30-40%. Furthermore, the tendency of all the models to underestimate observed $[ClO]/[ClONO_2]$ (assuming model-measurement agreement for $[NO_2]$) results in [ClO] estimates that are in deceptively good agreement with the POLARIS observations.

In summary, our results suggest means of improving both the accuracy and precision of photochemical models. Changes will tend to shift modeled inorganic chlorine partitioning toward HCl and, to a lesser degree, reduce ClO concentrations in simulations of the gas-phase lower stratosphere.

Acknowledgments. We thank NASA's Upper Atmosphere Research Program as well as the researchers, pilots, crew, and managers of NASA's ER-2 program for supporting the POLARIS campaign. This work was funded under NASA grants NAG-1-2007 and NAG-2-1300. We thank J. J. Margitan for the ER-2 O_3 data. P. B. Voss is grateful for support from NASA's Global Change Fellowship Program.

References

Battin-Leclerc, F., I.K. Kim, and R.K. Talukdar, Rate coefficients for the reactions of OH and OD with HCl and DCl between 200 and 400 K, *J. Phys. Chem. A*, *103*, 3237-3244, 1999.

Bonne, G.P., et al., An examination of the inorganic chlorine budget in the lower stratosphere, *J. Geophys. Res.*, *105*, 1957-1971, 2000.

Brown, S.S., R.K. Talukdar, and A.R. Ravishankara, Rate constants for the reaction $OH+NO_2+M$ to HNO_3+M under atmospheric conditions, *Chem. Phys. Lett.*, *299*, 277-284, 1999.

Brune, W.H., and J.G. Anderson, In situ observations of ClO in the Antartic: ER-2 aircraft results from 54°S to 72°N latitude, *J. Geophys. Res.*, *94*, 16,649-16,663, 1989.

Cohen, R.C., et al., Quantitative constraints on the atmospheric chemistry of nitrogen oxides: An analysis along chemical coordinates, *J. Geophys. Res.*, in press, 2000.

Del Negro, L.A., et al., Comparison of modeled and observed values of NO_2 and J_{NO2} during the Photochemistry of Ozone Loss in the Arctic Region in Summer (POLARIS) mission, *J. Geophys. Res.*, *104*, 26,687-26,*704*, 1999.

DeMore, W.B., Tests of stratospheric models: The reactions of atomic chlorine with O_3 and CH_4 at low temperature, *J. Geophys. Res.*, *96*, 4995-5000, 1991.

DeMore, W.B., S.P Sander, D.M. Golden, R.F. Hampson, M.J. Kurylo, C.J. Howard, A.R. Ravishankara, C.E. Kolb, and M.J. Molina, Chemical kinetics and photochemical data for use in stratospheric modeling, Evaluation number 12, *JPL Publ.*, *97-4*, 1997.

Dessler, A.E., et al., Correlated observations of HCl and $ClONO_2$ from UARS and implications for stratospheric chlorine partitioning, *Geophys. Res. Lett.*, *22*, 1721-1724, 1995.

Dransfield, T.J., K.K. Perkins, N.M. Donahue, and J.G. Anderson, Temperature and pressure dependent kinetics of the gas-phase reaction of the hydroxyl radical with nitrogen dioxide, *Geophys. Res. Lett.*, *26*, 687-690, 1999.

Elkins, J.W., et al., Airborn gas chromatograph for long-lived species in the upper troposphere and lower stratosphere, *Geophys. Res. Lett.*, *23*, 347-350, 1996.

Fahey, D.W., D.M. Murphy, K.K. Kelly, M.K.W. Ko, M.H. Proffitt, C.S. Eubank, G.V. Ferry, M. Lowenstein, and K.R. Chan, Measurements of nitric oxide and total reactive nitrogen in the Antarctic stratosphere: Observations and chemical interpretations, *J. Geophys. Res.*, *94*, 16,665-16,681, 1989.

Fahey, D.W., et al., In situ observations of NO_y, O_3, and the NO_y/O_3 ratio in the lower stratosphere, *Geophys. Res. Lett.*, *23*, 1653-1656, 1996.

Gao et al., A comparison of observations and model simulations of NO_x/NO_y in the lower stratosphere, *J. Geophys. Res. Lett.*, 26, 1153-1156, 1999

Golub, G.H., and J.M. Ortega, *Scientific Computing and Differential Equations: An Introduction to Numerical Methods*, pp. 61-64, Academic, San Diego, Calif., 1992.

Gunther, A., B. Levrat, and H. Lipps, International Computing Symposium 1973, paper presented at the *International Computing Symposium 1973*, Davos, Switzerland, The European Chapters of the Association for Computer Machinery, Sept. 1973.

Hanisco, T.F., et al., Sources, sinks, and the distribution of OH in the lower stratosphere, *J. Phys. Chem.*, in press, 2001.

Kegley-Owen, C.S., M.K. Gilles, and J.B. Burkholder, Rate coefficient measurements for the reaction OH+ClO→products, *J. Phys. Chem. A*, *103*, 5040-5048, 1999.

Lipson, J.B., M.J. Elrod, T.W. Beiderhase, L.T. Molina, and M.J. Molina, Temperature dependence of the rate constant and branching ratio for the OH+ClO reaction, *J. Chem. Soc. Faraday Trans.*, *93*, 2665-2673, 1997.

Liu, X., R.D. Blatherwick, and F.J. Murcray, Measurements and model calculations of the HCl column amounts and related species over McMurdo during the austural spring of 1989, *J. Geophys. Res.*, *97*, 20,795-20,804, 1992.

McElroy, C.T., A spectroradiometer for the measurement of direct and scattered solar irradiance from on-board the NASA ER-2 high altitude research aircraft, *Geophys. Res. Lett.*, *22*, 1361-1364, 1995.

Michelsen, H.A., et al., Stratospheric chlorine partitioning: Constrains from shuttle-borne measurements of [HCl], [$ClONO_2$], and [ClO], *Geophys. Res. Lett.*, *23*, 2361-2364, 1996.

Nevison, C.D., S. Solomon, and R.S. Gao, Buffering interactions in the modeled response of stratospheric O_3 to increased NO_x and HO_x, *J. Geophys. Res.*, *104*, 3741-3754, 1999.

Nicovich, J.M., K.D. Kreutter, and P.H. Wine, Kinetics of the reactions of $Cl(^2P_J)$ and $Br(^2P_{3/2})$ with O_3, *Int. J. Chem. Kinet.*, *22*, 399-414, 1990.

Osterman, G.B., B. Sen, G.C. Toon, R.J. Salawitch, J.J. Margitan, J.F. Blavier, D.W. Fahey, and R.S. Gao, Partitioning of NO_y species in the summer arctic stratosphere, *Geophys. Res. Lett.*, *26*, 1157-1160, 1999.

Payan, S., C. Camy-Peyret, P. Jeseck, T. Hawat, G. Durry, and F. Lefevre, First direct simultaneous HCl and $ClONO_2$ profile measurements in the Arctic vortex, *Geophys. Res. Lett.*, *25*, 2663-2666, 1998.

Perkins, K.K., R.C. Cohen, L.B. Lapson, P.O. Wennberg, L.C. Koch, N.T. Allen, J.N. Demusz, J.F. Oliver, R.M. Stimpfle, and J.G. Anderson, NO_2 detection by laser-induced fluorescence: A new technique for in situ measurements of NO_2 in the lower stratosphere, *J. Phys. Chem.*, in press, 2001.

Portmann, R.W.., S.S. Brown, T. Gierczak, R.K. Talukdar, J.B. Burkholder, A.R. Ravishankara, Role of nitrogen oxides in the stratosphere: A reevaluation based on laboratory studies, *Geophys. Res. Lett.*, *26*, 2387-2390, 1999.

Prather, M.J., Ozone in the upper stratosphere and mesosphere, *J. Geophys. Res.*, *86*, 919-939, 1981.

Prather, M.J., Lifetimes and eigenstates in atmospheric chemistry, *Geophys. Res. Lett.*, *21*, 801-804, 1994.

Press, W.H., B.P. Flannery, S.A. Teukolsky, and W.T. Vetterling, *Numerical Recipes in C: The Art of Scientific Computing*, pp. 255-289, Cambridge Univ. Press, New York, 1988.

Proffitt, M.H., and R.J. McLaughlin, Fast-response dual-beam UV absorption ozone photometer suitable for use on stratospheric balloons, *Rev. Sci. Instrum.*, *54*, 1719-1728, 1983.

Rinsland, C.P., R. Zandler, C.B. Farmer, R.H. Norton, and J.M. Russel III, Concentrations of ethane (C_2H_6) in the lower stratosphere and upper troposphere and acetylene (C_2H_2) in the upper troposphere deduced from Atmospheric Trace Molecule Spectroscopy/Spacelab 3 spectra, *J. Geophys. Res.*, *92*, 11,951-11,964, 1987.

Rowland, F.S., J.E. Spencer, and M.J. Molina, Estimated relative abundance of chlorine nitrate among stratospheric chlorine compounds, *J. Phys. Chem.*, *80*, 2713-2715, 1976.

Salawitch, R.J., et al., The distribution of hydrogen, nitrogen, and chlorine radicals in the lower stratosphere: Implications for changes in O_3 due to emission of NO_y from supersonic aircraft, *Geophys. Res. Lett.*, *21*, 2547-2550, 1994a.

Salawitch, R.J., et al., The diurnal variation of hydrogen, nitrogen, and chlorine radicals: Implications for heterogeneous production of HNO_2, *Geophys. Res. Lett.*, *21*, 2551-2554, 1994b.

Sander, S.P., et al., Chemical kinetics and photochemical data for use in stratospheric modeling, Evaluation number 13, *JPL Publ. 00-3*, 2000.

Scott, S.G., T.P. Bui, K.R. Chan, and S.W. Bowen, The meteorological measurement system on the ER-2 aircraft, *J. Atmos. Ocean. Technol.*, *7*, 525-540, 1990.

Schubert, S. D., R. R. Rood, and J. Pfaendtner, An assimilated data set for earth sciences applications, *Bull. Am. Meteorol. Soc.*, *74*, 2331-2342, 1993.

Sen, B., B.B. et al., The budget and partitioning of stratospheric chlorine during POLARIS, *J. Geophys. Res.*, *104*, 26,653-26,665, 1999.

Stimpfle, R.M., et al., The coupling of $ClONO_2$, ClO, and NO_2 in the lower stratosphere from in situ observations using the NASA ER-2 aircraft, *J. Geophys. Res.*, *104*, 26,705-26,715, 1999.

Swartz, W.H., S.A. Lloyd, T.L. Kusterer, D.E. Anderson, C.T. McElroy, and C. Midwinter, A sensitivity study of photolysis rate coefficients during POLARIS, *J. Geophys. Res.*, *104*, 26,725-26,736, 1999.

Toon, G.C., et al., Comparison of MkIV balloon and ER-2 aircraft measurements of atmospheric trace gases, *J. Geophys. Res.*, *104*, 26,779-26,790, 1999.

Toumi, R., R.L. Jones, and J.A. Pyle, Stratospheric ozone depletion by $ClONO_2$ photolysis, *Nature*, *365*, 37-39, 1993.

Webster, C.R., R.D. May, D.W. Toohey, L.M. Avallone, J.G. Anderson, and S. Solomon, In situ measurements of the ClO/HCl ratio: Heterogeneous processing on sulfate aerosols and polar stratospheric clouds, *Geophys. Res. Lett.*, *20*, 2523-2526, 1993.

Webster, C.R., et al., Hydrochloric acid and the chlorine budget of the lower stratosphere, *Geophys. Res. Lett.*, *21*, 2575-2578, 1994a.

Webster, C.R., R.D. May, C.A. Trimble, R.G. Chave, and J. Kendall, Aircraft (ER-2) Laser Infrared-Absorption Spectrometer (ALIAS) for in-situ measurements of HCl, N_2 O, CH_4, NO_2, and HNO3, *Appl. Opt.*, *33*, 454-472, 1994b.

Webster, C.R., et al., Evolution of HCl concentrations in the lower stratosphere from 1991 to 1996 following the eruption of Mt. Pinatubo, *Geophys. Res. Lett.*, *25*, 995-998, 1998.

Wennberg, P.O., et al., Removal of stratospheric O_3 by radicals: In situ measurements of OH, HO_2, NO, NO_2, ClO, and BrO, *Science*, *266*, 398-404, 1994a.

Wennberg, P.O., R.C Cohen, and N.L Hazen, L.B. Lapson, N.T. Allen, T.F. Hanisco, J.F. Oliver, N.W. Lanham, J.N. Demusz, and J. G. Anderson, Aircraft-borne laser-induced fluorescence instrument for the in situ detection of hydroxyl and hydroperoxyl radicals, *Rev. Sci. Instrum.*, *65*, 1858-1876, 1994b.

Wennberg, P.O., et al., Twilight observations suggest unknown sources of HO_x, *Geophys. Res. Lett.*, *26*, 1373-1376, 1999.

G. Bonne, Applied Materials, 3050 Bowers Avenue, Santa Clara, CA, 95054.

T. P. Bui, NASA Ames Research Center, Moffett Field, CA 94035.

R. Cohen, Department of Chemistry and Department of Geology and Geophysics, University of California, Berkeley, CA 94720.

J. W. Elkins, NOAA Climate Monitoring and Diagnostics Laboratory, Boulder, CO, 80303.

P. A. Newman and L. R. Lait, NASA Goddard Space Flight Center, Greenbelt, MD, 20771.

R. Salawitch, C. Webster, D. Scott, and R. May, Jet Propulsion Laboratory, California Institute of Technology, Pasadena, CA 91125

P. Voss, R. Stimpfle, T. Hanisco, K. Perkins, E. Lanzendorf, J. Anderson, Department of Chemistry and Chemical Biology, Harvard University, Cambridge, MA 02144. (p_voss@huarp.harvard.edu; hanisco@huarp.harvard.edu;perkins@huarp.harvard.edu;lanzendorf @huarp.harvard.edu;anderson@huarp.harvard.edu.)

P. O. Wennberg, Division of Geological and Planetary Sciences, California Institute of Technology, Pasadena, CA 91125.

(Received March 14, 2000; revised July 24, 2000;
accepted August 8, 2000.)